Chem Soc Rev

REVIEW ARTICLE

View Article Online
View Journal

Cite this: DOI: 10.1039/c8cs00543e

Waste-to-wealth: biowaste valorization into valuable bio(nano)materials

Chunping Xu,†[a] Mahmoud Nasrollahzadeh, †*[b] Maurizio Selva, *[cd] Zahra Issaabadi[b] and Rafael Luque *[de]

Received 13th March 2019

DOI: 10.1039/c8cs00543e

rsc.li/chem-soc-rev

The waste-to-wealth concept aims to promote a future sustainable lifestyle where waste valorization is seen not only for its intrinsic benefits to the environment but also to develop new technologies, livelihoods and jobs. Based on the concept of waste valorization and circular economy, this review aims to provide an overview of present trends and future potential in the conversion of residues from different food sectors into valuable bio(nano)materials.

[a] School of Food and Biological Engineering, Zhengzhou University of Light Industry, Dongfeng Road 5, Zhengzhou, Henan 450002, P. R. China
[b] Department of Chemistry, Faculty of Science, University of Qom, Qom 3716146611, Iran. E-mail: mahmoudnasr81@gmail.com
[c] Dipartimento di Scienze Molecolari e Nanosistemi, Universita Ca Foscari, Via Torino 155, Venezia Mestre, 30175, Italy. E-mail: selva@unive.it
[d] Departamento de Quimica Organica, Universidad de Cordoba, Campus de Rabanales, Ctra Nnal IV-A, Km 396, E14014, Cordoba, Spain. E-mail: rafael.luque@uco.es
[e] Peoples Friendship University of Russia (RUDN University), 6 Miklukho Maklaya str., 117198, Moscow, Russia
† Equal contribution status.

1. Introduction

In the past century, the development of anthropic activities has resulted in a massive energy demand and consumption of resources which has had a serious impact on our planet's ecosystems and biodiversity, mostly through the release of waste in the different environmental compartments including biota, air, water, land and aquatic sediments. The high rate of increase in world population and the per capita needs have further accentuated the problem, making residues of industrial

Chunping Xu

Chunping Xu obtained his bachelor's degree in 2000 from the Department of Life Science, Henan Normal University, China, and master's degree in 2003 from the Department of Biotechnology, Daegu University, Korea. After his graduation, he worked as a researcher in the Department of Biological Functions and Engineering, Kyushu Institute of Technology, Japan. In 2005, he joined the University of Groningen, Faculty of Medicine, The Netherlands, where he finished his PhD studies in 2008 from the Department of Biomedical Engineering. Then, he went to work as a scientist in Philip Morris International R&D, Switzerland. Since 2010, he has been working in the School of Food and Biological Engineering, Zhengzhou University of Light Industry, China, as a professor. Dr Xu has a wide experience in natural products, biotransformation and food processing. He has produced more than 150 publications in the journals with significant impact factors.

Mahmoud Nasrollahzadeh

Mahmoud Nasrollahzadeh was born in 1981 in Iran. He received his PhD in Organic Chemistry from the Bu-Ali Sina University in 2012. He joined the University of Qom in 2013, where he developed new processes in organic synthesis and in homogeneous and heterogeneous catalysis. In 2016, he chaired one national conference and helped create the Center of Environmental Researches, a National Centre of Excellence for the regional problems of dusts. His research interests are new processes and scale-up in organic chemistry, organometallic catalysis, heterogeneous (nano)catalysis, phyto-chemistry and biomass/waste valorization. He is a member of the editorial board of several international journals, has published over 160 scientific papers, 9 reviews, 3 book chapters, 1 book in Elsevier, 1 patent and has edited 1 book.

production a global issue from both economic and ecologic/social standpoints because of disposal costs, hazard to human health, land use for storage, land and water pollution, climate change, *etc.* To cite only a few numbers, over 8 million tonnes of plastic are thrown away into the oceans each year and in 2017, the seas were polluted with almost 5 trillion pieces of plastic.[1]

Pertinent to this context and strictly consequential to human activities is also the generation of biodegradable residues or biowastes (BW) whose nature, however, is not yet unambiguously defined. The European Commission has proposed to include garden and park waste, food processing and kitchen waste from households, restaurants, caterers and retail premises, and food plants,[2] while on a more general basis, the literature expands the class of BW to domestic and sewage wastes, manure, food wastes and residues from forestry, agriculture and fisheries.[3] Whichever the classification, BW represent an enormous amount of organic and inorganic matter: the World Bank has estimated that by 2025, municipal solid wastes (only a part of BW) of the urban areas worldwide may reach 2.2 billion tonnes per annum, and waste generation rates might double over the next two decades in developing countries.[4]

The most common disposal methods of biowastes include microbial decomposition under either aerobic or anaerobic conditions, thermal degradation and sending to landfill. In recent years, the potential of BW has received increasing attention by academic and industrial communities aiming to identify strategies to convert low-value waste into new materials and products, and concurrently, developing technological and business models based on waste-to-value enterprises by the integration of biowaste processing within biorefinery schemes has been described.[5,6] In this respect, fish/shrimp waste, fly ash, lignocellulosic food derived waste, pig bristles, cattle manure and household waste are becoming model examples of BW (Fig. 1).

The vast generation, pervasive presence and chemical richness of such residues are contributing to make their valorization one of the most promising perspectives for both an effective reduction of the environmental impact of BW and economic profit. The following section summarizes some properties and potential of these residues.

Fish/shrimp waste (F/SW)

The impressive growth of per capita fish consumption from 12.6 kg in the early 1970s up to 19.8 kg in the early 2010s has pushed the United Nations' 2030 Agenda for Sustainable

Maurizio Selva

Maurizio Selva is a Full Professor of Organic Chemistry at the Department of Molecular Sciences and Nanosystems, University Ca' Foscari Venezia (Italy). Since the beginning of his academic career in the early 90s, his main research interests have been focused on the implementation of eco-friendly organic syntheses based on clean reagents, catalysts and solvents. More specifically, the development of green catalytic techniques for the upgrading of bio-based platform chemicals using dense CO_2 and dialkyl carbonates and multiphase systems assisted by ionic liquids are among the current topics of research of Prof. Selva.

Zahra Issaabadi

Zahra Issaabadi received her MSc in organic chemistry from the University of Qom in 2017 under the supervision of Dr Mahmoud Nasrollahzadeh on the use of biosynthesized nanocomposites, polymer supported metal complexes and ionic liquid based tetrazole. Recently, she started her PhD in Polymer Chemistry at the Iran Polymer and Petrochemical Institute (IPPI).

Rafael Luque

Rafael Luque (PhD in 2005 from Universidad de Cordoba, Spain) has significant experience on biomass and waste valorization practices to materials, fuels and chemicals as well as nanoscale chemistry (400+ publications, h-index 70, >21 000 citations, 5 patents, 10 edited books) as well as numerous contributions to book chapters and invited, guest, keynote and plenary lectures in scientific events worldwide. Prof. Luque is Editor-in-chief of Molecular Catalysis, and is also serving in the Advisory/Editorial Board of over 10 Q1 RSC, Wiley, ACS and Elsevier Journals. Prof. Luque was named 2018 Highly Cited Researcher (Clarivate Analytics) and is currently Director of the Center for Molecular Design and Synthesis of Innovative Compounds for Medicine at RUDN University in Moscow, Russia, and Chair Professor at Xi'an Jiaotong University in China.

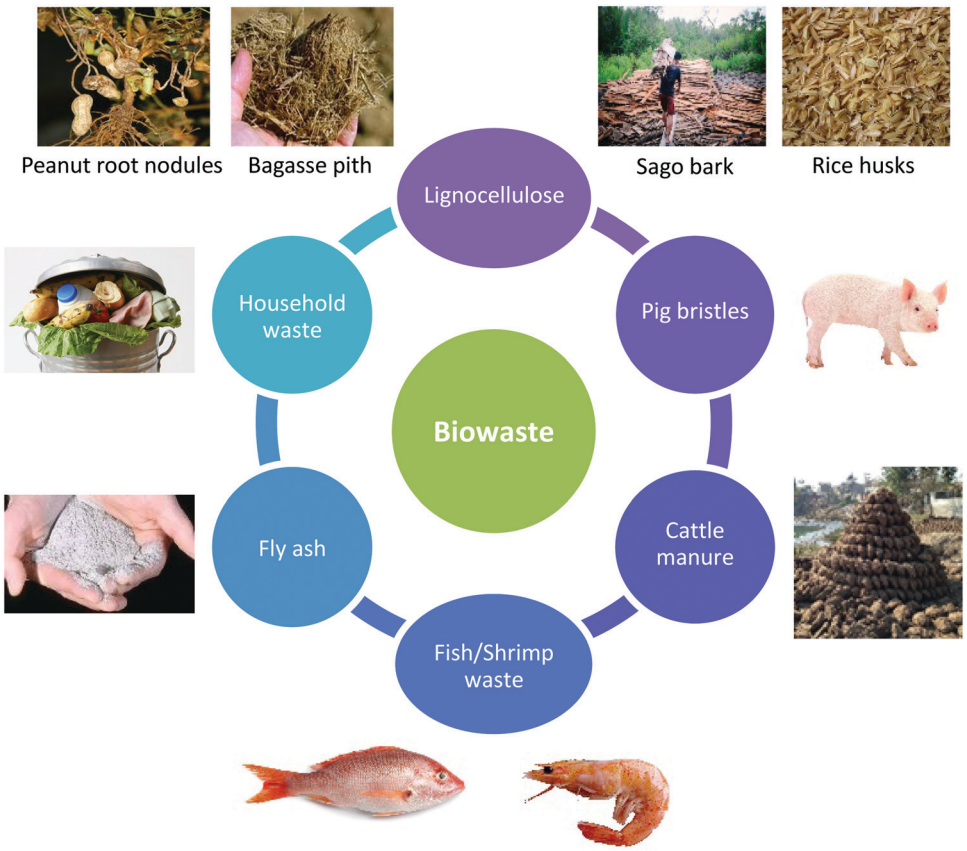

Fig. 1 Most common and widely available biowaste feedstocks.

Development and FAO (Food and Agriculture Organization of the United Nations) to recognize not only the primary role of fisheries and aquaculture in food security and nutrition, but also the need to reduce fishing beyond biological sustainability, and improve the recovery and upgrading of wastes.[7–9] This is imperative to lower the impact of the anthropic exploitation of marine resources and preserve coastal environments. According to recent findings, fishery waste accounts for over 20 million tonnes per year which corresponds approximately to 25% of the total production including by-catch (''non-target'' species) and fish processing waste.[10,11] Fish residues are comprised of whole waste fish, fish heads, skin, viscera, blood, bones, gonads, frame liver, guts, some muscle tissue, *etc.* and represent a source of several potentially valuable molecules including oils, proteins, pigments, bioactive peptides, amino acids, collagen, chitin, gelatin, *etc.*,[12] for the recovery/upgrading of which, many processes and technologies have been reported in the past decade or so.[13,14] Yet, there is still a way to go for large scale implementation. Of the major issues with F/SW, other than the unpleasant odor, the highly variable degradation times must be mentioned. Organic fish waste rapidly decomposes in hours or days according to environmental conditions, while exoskeletons of shrimps and crustaceans are extremely stable and recalcitrant to chemical or enzymatic breakdown.[15] This implies significant differences along the treatment/valorization chain of fish residues and side streams, dealing with their transport, storage and delivery to biorefining operations. This problem has been addressed through specific actions within Horizon 2020, the biggest EU research and innovation programme.[16]

The use of side products reduces the cost of waste disposal and generates additional revenues, being a good opportunity for cleaner production in industry. The fish and seafood industry produces large quantities of stinky waste, which causes environmental, social and economic problems. However, marine waste can contain added value substances including biopolymers.[17,18] Turning waste into wealth is a rather innovative and potentially economical approach towards value added products. For example, one of the most important challenges in absorption processes is the high cost of activated carbon production, which has led to a focus on providing solutions to reduce costs. Recently, solutions have been proposed regarding low cost alternative methods from the environmental, social and economic points of view. The use of shrimp and seafood waste to produce activated carbon can be a promising alternative to reduce environmental pollution and waste management costs.[19,20]

Furthermore, the preparation of chitosan and chitin from fishing industry waste (crustacean wastes) has proved to be economically attractive and environmentally feasible, especially when it involves the recovery of carotenoids.[21] In addition, shrimp head silage powder as a waste product from the shrimp export industry can be used as a substitute good quality protein

source for fish flour with economic advantages and without sacrificing the feed quality.[22]

Fly ash

Fly ash is traditionally referred to as the main inorganic by-product from the combustion of pulverized coal in power plants, and comprises a mixture of unburned carbon and inorganic oxides including hematite, lime, silica, alumina, potassium oxide, titania and magnesium oxide.[23] As such, fly ash from coal (CFA) is not a biowaste. However, in the search for alternative energy over the past fifteen years, several technologies have been developed based on co-firing biomass, including residues of the forest industry and agricultural wastes from cereal production and oil extraction factories, with coal.[24–26] Mixtures of coal with up to 20 wt% of residual biomass have been used, generating the so-called co-combustion fly ash (CCFA). This practice allows a more economical and environmentally benign application of coal with reduced pollutant emissions.[27] Although biomass can also be individually combusted in power plants, two considerable challenges are the lower heating value and corrosivity (due to the salt content) of bio-residues. A technology to cope with these problems has been recently proposed by burning wood biomass (pellets, chips and sawdust) in the presence of low-alkali CFA ($\leq$4 wt%).[28] The by-product of this combustion process has been named coal bio ash (CBA). Notably, it has been demonstrated that CBA can be a better alternative for cement in comparison with CFA. Applications of fly ash have been extensively reviewed in recent years: favorable physicochemical characteristics, such as sphericity of particles, porosity, light texture, low bulk density, and high surface area, account for the use of fly ash in a plethora of fields, such as additives for construction and ceramic materials, catalysts, solids for soil and water remediation and recovery of precious metals, *etc.*[29,30] In this respect, technology transfer to biomass fly ash has been recommended not only for its potential in reducing CO_2 emission,[31] but also for its benefits especially as an additive to increase the porosity and lower the density of microstructures in concrete.

Generally, the advantages of the use of fly ash include

- Space saving for disposal and natural resources
- Environmental protection and energy savings

The use of fly ash in various fields has been considered due to a potential reduction in the cost of raw materials and production.[32–34] Some of the most important examples in this area include carbon nanotubes (CNTs),[35] carbon nanofibers[36] and carbon nanomaterials (CNMs)[37] which have a costly production process due to the use of expensive catalysts and precursors. Economic issues in the production of CNTs limit their potential use in composite products. Since fly ash is practically free, its application as a catalyst can be potentially relevant to deal with these economic issues.

Lignocellulose (LC)

Lignocellulose is the most abundant renewable biomass on earth with an estimated global production of about 181.5 billion tonnes per year.[38] Most of this material is involved in the natural carbon cycle of terrestrial ecosystems, undergoing microbial decomposition and transformations which ultimately afford CO_2 and water. However, a significant portion of LC generates biowaste, mostly coming from forestry and agricultural industries, which are promising sources for energy, chemicals, materials and food thanks to the content of phenolics, polysaccharides, and proteins.[39–42] Major challenges of lignocellulosic biorefineries (LCB) come from the strong interactions occurring between LC-components (lignin, cellulose and hemicellulose), which depend on the lignin content, crystallinity of cellulose, and particle size, and make this biomass a highly resistant and recalcitrant structure.[43] The key to the success of LCBs largely relies on effective fractionation pre-treatments of feedstocks to separate LC-components and allow their further processing into biofuels and biochemicals. Of the multiple methods developed for LC deconstruction, current technologies mostly exploit thermochemical conversion such as enzymatic hydrolysis, hydrothermal liquefaction, acid and alkaline hydrolysis, ammonia fiber expansion, steam explosion, and mechanical milling; however, other less energy demanding procedures are emerging based on extrusion and dissolution in ionic liquid solvents.[44–49]

In large industrial plants, attention must be paid to environmental pollution and economic efficiency. The use of lignocellulose as one of the most renewable sources has become an active research field, potentially able to provide economic, social and environmental benefits.[50] There are several reports on the production of bioethanol and valuable chemicals from lignocellulosic biomass.[51] Lignocellulosic ethanol is a potential green and sustainable alternative transportation fuel.[52,53] On the other hand, the major components of lignocellulose are cellulose (35–50%), hemicellulose (20–30%) and lignin (10–25%). According to the literature, cellulose, hemicellulose and lignin can be converted to soluble pulp for the production of textile fibers and chemicals, furfural as a valuable platform chemical and carbon products (carbon foam, fibers and battery anodes), respectively.[54]

Pig bristles

Today, technology development has enabled the transformation of high cost waste into high value-added products which are environmentally sustainable and cost effective. Pig bristles are low value bio-residues, which can be converted into high value bio-based products by means of environmentally friendly technologies. In 2013 only, pork meat processing co-generated approximately 222 thousand tons of wet pig bristles and hooves in the EU, with disposal costs estimated to be slightly over four million Euros.[55] Although pig bristles consist of 90% or more of valuable protein such as keratin, digestibility of this biowaste is rather challenging because the protein is packed with fibres cross-linked by multiple disulfide bonds which confer exceptional stability towards common proteolytic enzymes such as pepsin, trypsin and papain.[56,57] Notably, a promising technology is currently being developed in the Danish project keratin2protein,[58] by which tailor-made microbial consortia cultivated in an industrial process are used for the degradation of keratin into a protein enriched product which has been proposed as an alternative

high-value feed for fish. This (sustainable) approach is under study to partly relieve issues posed by the global demand of aquaculture feed that is estimated to reach 71 million tonnes by 2020, almost double compared to 2008, and ten-fold that of 1995.[39,59]

Cattle manure and derived waste

Cattle manure has been used as a soil fertilizer for centuries, and this is still a living practice all over the world. In addition to macro and micronutrients, the organic matter necessary for the health of agricultural soils is provided by manure. FAO has recently reported that considering only the nitrogen (N) inputs, global manure production from all livestock has increased by 66% (from 73 to 124 million tonnes of N) from 1961 to 2016, manure addition to soils has increased from 18 to 28 million tonnes of N, and N input from manure left on pasture has increased from 48 to 86 million tonnes of N.[60] However, cattle manure is one of the most fetid and less valuable animal debris, which causes many environmental problems. In other words, inappropriate manure management and excessive applications can also have detrimental effects on the environment, contributing to the contamination of water and soil resources and to increased greenhouse gas (GHG) emissions. However, the same waste can potentially be an additional source of revenues through simple processing methods to improve its palatability or direct re-feeding. A considerable interest has therefore developed towards anaerobic digestion (AD) of manure as an option to provide bio-methane for local energy needs in animal husbandry and farming.[61] Burning such biowaste to generate power and CO_2 may become a climate-neutral practice, meaning that it does contribute to mitigating the increase of GHG concentrations due to methane from unmanaged livestock residues.[62] It should be noted, however, that the low carbon to nitrogen (C/N) ratio in animal manure brings about a moderate yield of biogas, which often does not justify capital costs for farm-scale plants. Effective solutions to improve the overall (gas) productivity have been conceived through the introduction of carbon-rich co-substrates into the anaerobic digester.[63] Many examples have been reported of co-digestion of mixtures of manure containing agro- and lignocellulosic-wastes and energy crops (maize, grass, wheat straw, palm pressed fiber, whole stillage from fermentative processes, corn stover, algae, *etc.*), food wastes, and even crude glycerol from biodiesel manufacture.[62,64–68] Manure valorization has been explored also by other flexible technologies, in particular, hydrothermal liquefaction (HTL) to produce bio-oil (biocrude); regardless of the initial composition of residues, the resulting liquid needed further upgrading before it could be used as a transportation fuel.[69,70] Technological advances provided additional processing methods including chemical and mechanical treatments, anaerobic and aerobic production of protein biomass, oxidation ditch, and biochemical recycling processes for the use of cattle manure and derived waste.[71]

Household waste

The World Bank has estimated that in 2016, the release of solid household waste (HW) originated as discards from daily domestic activities in the worlds' cities amounted to a footprint of 0.74 kilograms per person per day.[72] HW, also known as residential waste or domestic waste, has a highly heterogeneous composition including not only C-rich organic materials such as food scraps, garden waste, paper mostly as cardboard and newspapers, and natural textiles, but also plastic and glass bottles and boxes, metals from cans, electronic waste (E-waste), *etc.* (Fig. 2). However, HW composition can be significantly different for various countries worldwide. In most cases, paper and organic materials (such as yard (grass, leaves, brush) waste, wood, food scraps, and process residues) are the main HW. HW composition is influenced by factors such as energy sources, climate, economic development, and culture, which generally point out how urban waste streams are richer in organic matter for low- and middle-income countries, ranging from 40 to 85% of the total, while the release of paper, plastic, glass, and metal fractions increases for high-income countries.[73] Table 1 illustrates three case studies exemplifying the disclosed scenarios. The data with respect to HW composition are approximate values generated per country.

The organic residues of HW, particularly food waste, make up the largest single waste type and often the most abundant fraction of the overall discards. Therefore, not surprisingly, research on HW-management strategies is frequently focused on the valorization of food wastes which belong to the general family of biowastes pertinent to the present paper.[77] This topic has been examined by some recent review papers that highlighted the following major aspects:[78–80] (i) although a generally accepted definition of food waste is still unknown and evaluations of the amounts produced are not yet consolidated, almost 1.3 billion tonnes per year, *i.e.* one-third of the food produced for human use, is wasted worldwide with contributions of 92.4, 90, 61, 6.2, 4, and 2 million tons per year from China, Europe, United States, South Korea, Australia, and Japan, respectively; (ii) efforts are presently being addressed on the upgrading of food waste to biofuels and bio-products. In this respect, most promising technologies for bioenergy production are based on transesterification of oils and fats to produce biodiesel, fermentation of carbohydrates to bio-ethanol or bio-butanol, anaerobic digestion to bio-methane (see also the previous paragraph), dark fermentation to produce hydrogen, pyrolysis and gasification to obtain oil and syngas, and hydrothermal carbonization to get hydrochar, while for the synthesis of bio-based molecules and materials, attention is focused on chemical, chemo-enzymatic, and biotechnological treatments of food waste to obtain mostly bio-monomers for polylactates and polyhydroxyalkanoates, succinic acid, furfural and furans, and phenolic compounds; (iii) case studies available so far highlight the potential of integrating sequential steps of food waste valorization within the biorefinery concept and application prospects are becoming increasingly close to realization as alternatives to residue disposal in landfills. Generally, household wastes constitute a large amount of waste, which upon valorization can reduce waste disposal costs/environmental issues and generate additional revenues in the form of materials or energy recovery.[81] In light of the above analysis and pressing need to reduce worldwide production of biodegradable residues and

Fig. 2 Types of household waste.

Table 1 Composition of household waste in model urban areas

		HW composition (% of waste fractions)						
Entry	Urban area	Food	Plastics	Paper	Glass	Metals	Misc.[a]	Ref.
1	Dehradun city, India	≥80	~7	~8[b]	~1[c]	na[d]	~4	74
2	Saudi Arabia, Coastal area	40–70	10–15	10–35	5–10	5–10	5–15	75
3	Scotland	23	32[e]	20	8	na[d]	17[f]	76

[a] Miscellaneous including cloths, silt, dirt, rubber. [b] Including cardboard. [c] Including ceramic scraps. [d] Not available. [e] Including mostly healthcare waste, plastic films and dense plastics. [f] Including only garden waste.

improve their management, this contribution as a tutorial review aims at providing an insightful definition of the valorization concept of biowaste.

2. Biowaste to biomaterials

Biomaterials are designed to engineer biomedical devices capable of replacing a part or a function of the human body. Due to their direct interaction with living organisms, biomaterials must combine stringent requisites of biocompatibility, pharmacological acceptability (nontoxicity, non-allergenicity, non-immunogenicity, *etc.*), mechanical strength, suitable weight and density, and cost-effectiveness.[82,83] The synthesis of such materials from both natural sources and biowastes is therefore a challenging area that is currently being investigated through several approaches. This section will overview the preparation of some representative biowaste derived materials.

2.1 Collagen and collagen-based biopolymers

Collagen is the most abundant fibrous protein found in animal and human bodies.[84] Among 29 different structures of collagen that have been identified, the most common ones are type I present in bones, skin, dermis, vasculature, tendons, ligaments, cornea, and organs, type II constituting cartilages, type III found in reticular fibers of most tissues, spleen, skin, lungs, and liver, type IV forming the basement membrane and basal lamina, and type V, which is associated with type I collagen, especially in the cornea. Collagen molecules are made up of three α-chains intertwined in the so-called collagen triple-helix (Fig. 3).[85]

The structure, basically stabilized by intra- and inter-chain hydrogen bonding, is produced by an almost continuous repetition of the Gly-X-Y sequence, in which X and Y are often proline and hydroxyproline, respectively. A different arrangement is instead, observed for the short N- and C-terminal portions of the structure. These segments, called telopeptides, do not form triple helical

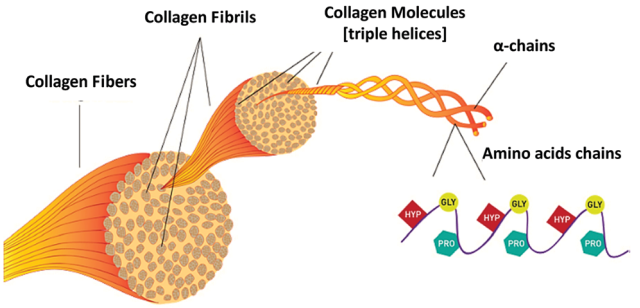

Fig. 3 Collagen structure. Adapted with permission from http://blog.nkdnutrition.com/collagen-synthesis/.

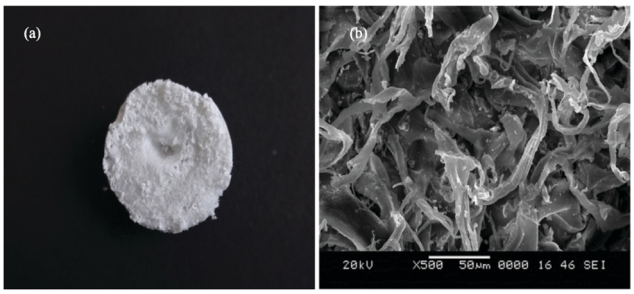

Fig. 5 Lyophilised collagen from sole fish skin: (a) as viewed by the naked eye and (b) SEM micrograph. Adapted from ref. 92. Copyright 2018, with permission from Elsevier.

structures, but are comprised of 15–26 amino acid residues mostly of lysine, hydroxylysine, and their aldehyde derivatives, which undergo intra- and inter-molecular covalent cross-linking forming the basic unit of collagen fibrils. The typical strong nature of skin, tendons and bones is caused by a network of cross-linked collagen fibrils.

Collagen exhibits remarkable bioactive properties, including biodegradability, non-immunogenicity, biocompatibility and low antigenicity, which account for its extensive use as a biomaterial in a variety of applications in medical, cosmetic, tissue engineering, and food sectors (Fig. 4).[86,87]

The different types of commercial collagens are obtained from a variety of animal connective tissues through extraction procedures based on acidic, alkaline, or neutral solubilization or enzymatic treatments. These processes, however, are rather expensive due to the moderate extraction yields and/or partial degradation of the product collagen. For example, enzymatic breakdown may cleave the terminal cross-linked portion of collagen, producing weak living tissue equivalents.[88] In the search for methods that improve yields and compositions, the use of biowastes, especially the organic fraction of fish discards (see above), has been explored as a low cost and ecofriendly source of collagen. The first studies in this field date back to over 20 years ago,[89,90] but recent developments are attracting increasing attention also for large scale production. Among them, an interesting procedure has been designed starting from defatted samples of flatfish skin which were treated in acetic acid (0.05 M; 1 : 100, sample : acetic acid, w/v) and extracted by using an industrial ultrasonication system of 8 L operating at 20 kHz. After 4.5 h at 4 °C, the collagen yield was up to 46%, twice as high as that achieved by conventional methods.[91] The extract was proved to be native type I collagen. Another successful protocol was implemented starting from sole fish skin using a response surface methodology (RSM) with Box–Behnken design (BBD).[92] The collagen yield was optimized up to a maximum of 19.27 ± 0.05 mg g^{-1} of fish skin, obtained under specific conditions (0.54 M acetic acid, 1.90 M NaCl, 8.97 mL g^{-1} solvent/solid ratio and 36 h). SEM analysis proved that the extract was in the form of fibrils with irregular linkages, displaying large porosity suitable for the incorporation of chemicals and drugs (Fig. 5).

Collagen has been extracted also from waste fish scales using ionic liquids in which the activity coefficients (AC) of collagen were evaluated through a COSMO-RS computational approach.[93] The best solvent was identified as 1-ethyl-3-methylimidazolium acetate ([C_2C_1im][Ac]) for its low AC (inverse of solubility) and best fit Sigma profile. After pretreatment at 100 °C for 12 h, the extracted collagen was precipitated from the IL using NaCl solution (2 M) and eventually collected in a yield of 3.1 ± 0.5%.

Enzymatic digestion of fish residues was explored starting from aqueous suspensions comprised of defatted swim bladder waste (of rohu, an Indian major carp), and a mixture of acetic acid containing pepsin [EC 3.4.23.1; 3000–3500 NF U mg^{-1}; solid : liquid ratio of 1 : 10 (w/v)]. Pepsin soluble collagen (PSC) was achieved with 465.2 g kg^{-1} yield (dry weight basis). The enzymatic breakdown was performed at 4 °C for 48 h producing an extract that maintained the triple helical structure and showed a high fibril-forming ability.[94]

One last procedure mentioned here was devised through the application of a well-known technique in the food industry, *i.e.* extrusion. An innovative extrusion-hydro-extraction process was set up for the extraction of fish residues from tilapia fish scales (TFS).[95] The high pressure, high heat (135 °C), and high mechanical forces during the process acted synergistically to loosen chemical bonds between collagen and hydroxyapatite in

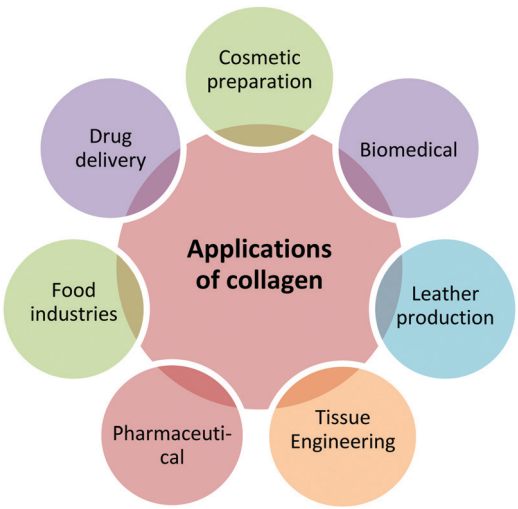

Fig. 4 Applications of collagen.

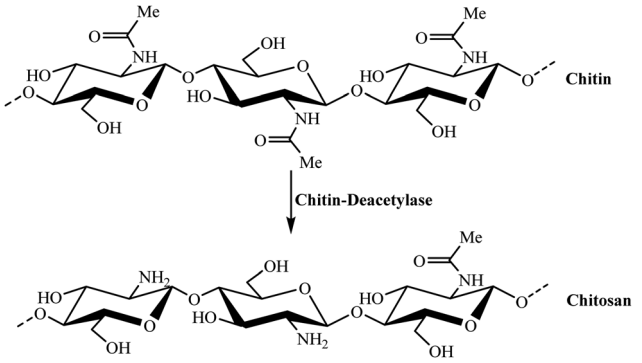

Fig. 6 Partial deacetylation of chitin (top) for the formation of chitosan (bottom).

fish scales, thereby providing type I collagen in yields up to 16 g protein/100 g crude protein content in TFS (dry basis). The method took advantage of typical benefits of the extrusion technique including continuous production, ease of operation, and little waste formation.

2.2 Chitin and chitosan derived biomaterials

Chitin and chitosan are natural aminopolysaccharides found together in nature.[96] The repeating units of chitin are comprised of β-(1–4)-2-acetamido-2-deoxy-β-D-glucose and β-(1–4)-2-deoxy-β-D-glucopyranose structures, respectively, producing poly(β-(1–4)-*N*-acetyl-D-glucosamine),[97] in a scaffold similar to that of cellulose (Fig. 6).

Indeed, chitin plays a role analogous to that of cellulose in plants and collagen in higher animals, existing as ordered crystalline microfibrils which form structural components in the arthropod and crustacean exoskeleton and fungal and yeast cell walls.

On the other hand, chitosan is the *N*-deacetylated derivative of chitin, a copolymer consisting of glucosamine and *N*-acetyl-glucosamine with a varying degree of acetylation (fraction of *N*-acetylated glycosidic units) typically less than 0.35 (Fig. 6). Chitosan formed by the enzymatic separation of acetyl groups from nascent chitin polymers, has been found as a significant part of the wall of fungal cells.[98]

Chitin. Crustacean wastes of the fishing industry are used to extract commercial chitin. The major sources are shrimp, crab, lobster, prawn and krill shells.[99–101] These biowastes usually contain chitin (20–30%), a protein portion (30–40%), inorganic salts, mainly calcium carbonate and phosphate (30–50%), and lipids (0–14%). Therefore, isolation of chitin generally requires consecutive steps of deproteinization, demineralization, and discoloration during which removal of protein and inorganic components is followed by the elimination of colored pigments (astaxanthin, canthaxanthin, astacene, lutein and β-carotene) typically present in crustaceans shells.[102] The deproteinization is carried out either chemically with diluted aq. NaOH solutions (1–10%) at 65–100 °C, or *via* biological fermentative treatments, while demineralization (removal of inorganic salts) takes place under diluted acid conditions with HCl, HNO_3, HCOOH, H_2SO_4, and CH_3COOH, and finally, discoloration is achieved at room temperature by solvent extraction mostly with acetone, ethanol, ethyl acetate or their mixtures. Crystalline chitin displays biocompatibility, biodegradability, antimicrobial activity, low immunogenicity, and eco-safety which makes it highly attractive in the field of biomaterials.[103]

Although the extended hydrogen bonded structure of chitin limits its solubility in most solvents, and consequently, its processing, new applications of chitin have been described in recent years, especially for the fabrication of nanomaterials. One such example is the synthesis of multi-functional hybrid bio-aerogels based on cellulose nanofibers (CNFs) decorated with chitin nanocrystals (CNCs).[104] Once CNFs and CNCs were extracted from corn husks and shrimp shells, respectively, an environmentally friendly freeze-drying process was devised during which a mixture comprised of an aqueous solution of CNFs with dispersed CNCs was first frozen at −73 °C in a dry ice–isopropanol bath and then freeze dried in a lyophilizer at −88 °C under vacuum for 4 days. FESEM images of three CNF aerogels with different amounts of CNCs (0, 1, and 2% referred to as neat AR, AR1 and AR2, respectively) are shown in Fig. 7 (left).

Increasing the amount of CNCs modified the morphology of the material particularly in AR2 (bottom) whose fiber orientation mimicked the multi-layer maple seed structure. CNCs showed a tendency to position themselves between the CNFs, reducing intermolecular interactions between fibers. This was consistent with the results obtained for removal of dyes (MB: methylene blue; Rh6G: rhodamine 6G) from aqueous solutions, which proved that AR2 was a far better adsorbent gel than neat AR and AR1. This behavior is explained by the mechanism of Fig. 7 (right), where interactions of positively charged dye molecules with acetamide-enriched AR2 favored adsorption (dotted lines). The multifunctional efficiency of AR2 was further confirmed by its superior antioxidant and antibacterial activities as compared to neat AR and AR1.

A similar concept was applied through a different approach for the synthesis of a layer-by-layer spray coating of cationic CNF and anionic CNC suspensions onto poly(lactic acid) (PLA) films.[105] Strong adsorption of thin alternating layers was herein promoted by the attractive electrostatic forces between CNFs and CNCs. However, self-repulsion between CNFs or CNCs in each layer led to more efficient packing. Therefore, films with a minimum of two alternating coated layers, composed of PLA–(CNC–CNF)*n*, showed significant reductions in O_2 permeability with respect to PLA alone, even at high relative humidity (RH = 70%). In terms of engineering applications, the potential of these films should be for a platform technology of 100% biorenewable barrier packaging, especially for foods, pharmaceuticals and electronics in which oxygen permeability is a key issue.

Other remarkable uses of chitin have been reported for the fabrication of nanofibers with diameters less than 100 nm.[106] Upon dissolving chitin in HFIP (hexafluoro-2-propanol), such materials were prepared through different methods including self-assembly, microcontact printing, and electrospinning. Chitin nanofibers with high molecular weight were successfully electrospun using 1-ethyl-3-methylimidazolium acetate as an ionic liquid solvent. Major applications of the fibers have been described in

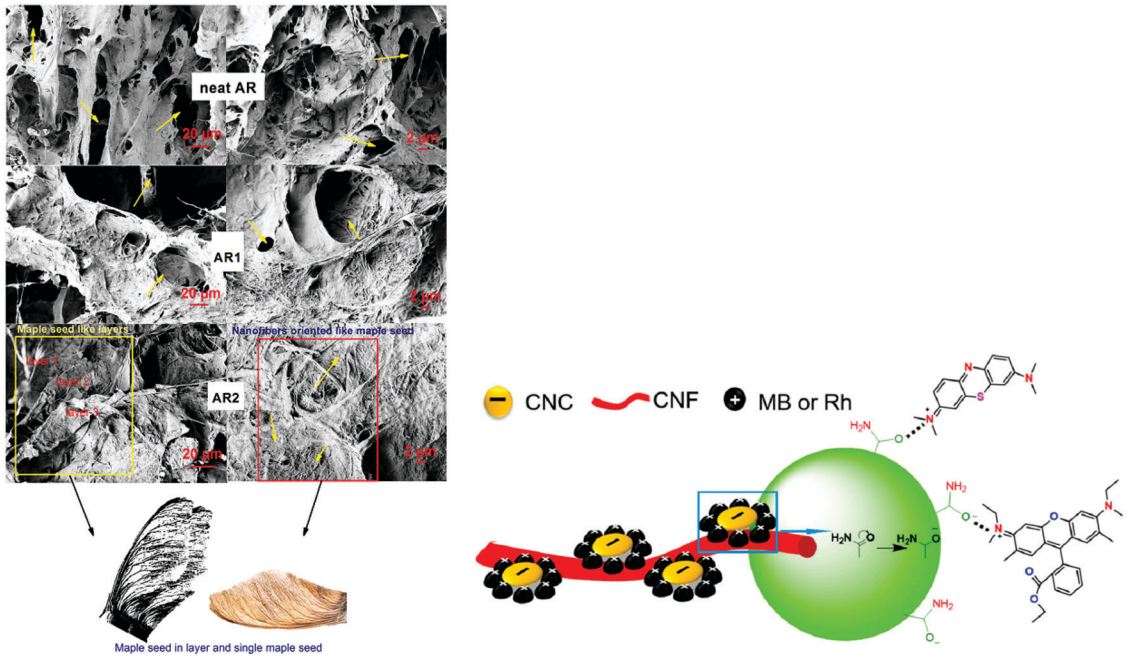

Fig. 7 Left: FESEM images of different aerogels; right: mechanism for adsorption of dyes (MB and Rh6G) into AR2. Adapted from ref. 104. Copyright 2017, with permission from the Royal Society of Chemistry.

tissue engineering mostly due to structure similarity to glycosaminoglycans in the native extracellular matrix (ECM).

Finally, chemical modifications have been reported to convert chitin into several derivatives such as, for example, N- and O-sulfonated chitin relevant for the similarity to heparin (blood anticoagulant), and dibutyryl- and carboxymethyl-chitin for biomedical applications in drug delivery.[107–109]

Chitosan. Chitosan is prepared by chitin deacetylation which involves alkaline hydrolysis of the acetamide groups of chitin. Hydrolysis procedures have been reported under heterogeneous conditions with a concentrated base (aq. NaOH, 40–50%; 100 °C) and an inert atmosphere to limit depolymerization, or under homogeneous conditions, at 25–40 °C, by freezing–pumping–thawing (FPT) cycles of an alkaline aqueous suspension of chitin until dissolution. The latter (homogeneous) deacetylation reaction is a more effective process involving moderate alkali concentrations ($\leq$13 wt%) and providing high-molecular weight chitosans with no chain compositional dispersion.[103]

A study examined the biological production of chitin achieved through lactic acid fermentation (LAF) of shrimp waste, and the subsequent deacetylation to chitosan.[110] Biological chitin (Bio-C) was obtained in a packed bed column reactor with maximal percentages of demineralization (D_{MIN}) and deproteinization (D_{PROT}) of 92 and 94%, respectively, after 96 h. The same shrimp waste was then subjected to acid/base chemical processing to get chemically extracted chitin (Ch-C). The comparison of the two methods proved that Bio-C had a higher crystallinity index (I_{CR}) (86%) and M_w (1200 kDa) than Ch-C. In the following step, the FPT deacetylation of Bio-C allowed one to obtain chitosan with a mid-range M_w (400 kDa) and an acetylation degree (DA) *ca.* 10% higher than that from Ch-C. The bio-chitosan showed a block copolymer structure inherited from the parent crystalline Bio-chitin. Overall, the biological protocol combining LAF and FPT procedures was effective to avoid both loss of crystallinity and excessive depolymerization in the chitosan product.

Another effective method for the preparation of chitosan from shrimp shells started with the usual deproteinization and demineralization processes followed by bleaching (discoloration) with ethanol. Thereafter, chitin was suspended in aq. NaOH (12.5 M), cooled down and kept frozen (24 h). The resulting chitosan obtained showed adequate physicochemical properties such as high solubility in acetic acid (1%), low ash content (0.063%), a molecular weight between 2.3 and 2.8 $\times$ 10^5 g mole^{-1}, a crystallinity index of around 40% and a deacetylation degree above 90%.[111]

Also, unconventional procedures for the deacetylation of chitin have been developed including thermomechanical processes, flash treatment under microwave dielectric heating, saturated steam, and intermittent water washings.[102] One such example was described for the preparation of low molecular weight chitosan (LMWC) through a solvent free, solid state mechanochemical method using chitin and crude shrimp shell powder.[112] In this approach, the simultaneous deacetylation and depolymerization of chitin was achieved using base catalysts under mechanochemical conditions. In comparison to multi-step procedures, this one-pot protocol showed advantages of increased efficiency, reduced environmental impact, reduced base consumption (to about 1/10), and narrow molecular weight distribution of the LMWC with a poly-dispersity value of only 1.1 (Fig. 8).

In contrast to the parent chitin, chitosan is readily soluble in dilute acids due to easy protonation of free amino groups. The pK_a (6.5) of these functions makes the polymer responsive to

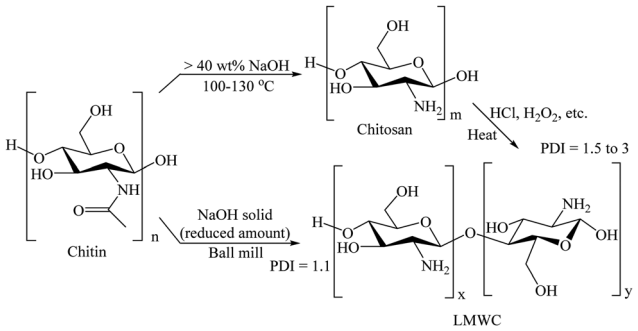

Fig. 8 A two-step traditional method (top) is compared to a one-step mechanochemical procedure (bottom). The used commercial chitin had a low DD value of 3.5% and the DD values of chitosan-C and chitosan-H were around 80%.

Fig. 9 Applications of chitosan.

acid/base conditions, acting as a protonated cationic polysaccharide below physiological pH. Accordingly, chitosan is far more accessible than chitin for both chemical reactions and other uses.[102,113] Fig. 9 summarizes the major fields of applications of chitosan.

Recently, antifungal and antibacterial activities of chitosan have been extensively reviewed,[99] concluding that several aspects may alter the behavior of the biopolymer. Chitosan presumably functions by electrostatic interactions between its positively charged protonated amino groups and the anionic parts of the cell surface. Hence, the degree of deacetylation (and availability of free amino functions) as well as the derivatization at N and O atoms in glucosamine units is crucial to modify the hydrophilicity/hydrophobicity balance of chitosan. Increased antifungal activity was found for both highly deacetylated and alkyl sulfonated chitosans, respectively. Quaternization reactions further improved the performance due to the permanent positive charge on N-atoms enhancing electrostatic interactions even at neutral pH. In addition, chitosans with a low molecular weight (LMW) in the range of 16–190 kDa seemed to be the most effective antifungal agents because they could easily penetrate the cell wall as compared to medium or high molecular weight homologues.

Other recent papers have highlighted an increasing number of applications of chitosan derived from residual crustacean shells. Among strategies to modify and improve the chitosan surface characteristics, atom transfer radical polymerization (ATRP) and graft copolymerization are emerging relevant techniques due to their compatibility with both aqueous and organic media and high tolerance against various functional groups.[114] ATPR was used to graft chitosan beads with polyacrylamide, or even more interestingly, to functionalize chitosan nanospheres (CTSNS) with poly(methylmethacrylate) (PMMA) and poly(methyl methacrylate)-*b*-poly(poly(ethylene glycol) methyl ether methacrylate) (PMMA-*b*-P(PEGMA)). Individual nanospheres consisting of a chitosan core and a densely grafted outer PMMA or PMMA-*b*-P(PEGMA) layer were produced (Fig. 10). Graft copolymers were potentially suitable for biomaterials.

The interaction of chitosan with both synthetic and natural polymers has been described also in the formation of polyelectrolyte complexes (PEC) and layer-by-layer polyelectrolyte capsules or films.[115] In this case, electrostatic forces stabilize the final material: examples were reported in which chitosan was coupled to lipidic vesicles for bioadhesives and permeabilizers, or anionic alginate for protein release.

Chitosan and its derivatives have found applications as eco-friendly coagulants/flocculants to remove charged particles from wastewater.[116] Polyethylene glycol (PEG)–chitosan and polyvinyl alcohol (PVA)–chitosan composites were reported to adsorb aqueous nitrate ions[117] with a capacity >50.68 mg g^{-1}, while the goethite/chitosan nanocomposite and carboxymethyl–chitosan were selective towards complexation of Pb(II), and Cd(II)/Cr(IV), respectively. Chitosan-based nanoparticles were also investigated to encapsulate and deliver bioactive compounds.[118] Prepared by either self-assembly or ionic gelation techniques, nanoliposomes derived from modified chitosan loaded with EGCG [(−)-epigallocatechin gallate, the major bioactive compound in green tea] and catechin-loaded chitosan nanoparticles proved extremely efficient for slow and controlled release of encapsulated polyphenols in the gastrointestinal tract. These studies are paving the way to exploit the antioxidant, anticancer, and antibacterial properties of (tea) polyphenols through new biomaterials suitable for oral administration, with better stability and penetrating action in intestinal mucus and with intestinal epithelial cell targeting properties.

2.3 Hydroxyapatite

Hydroxyapatite (HA) of the formula $Ca_{10}(PO_4)_6(OH)_2$ is one of the most significant compounds as a bone filler and scaffold for biomedical implants due to the similarity of its chemical composition to that of the mineral component of bone tissue and its bioactivity, biocompatibility, non-inflammatory behavior, and high osteoconductive and/or osteo-inductive non-toxicity (Fig. 11).[119]

Although synthetic hydroxyapatite (sHA) can be obtained from commercial phosphate salts through precipitation, hydrolysis, hydrothermal processes (sol–gel), and microwave-based procedures,[120] continuous effort is currently being made to valorise bioresources, and particularly biowastes, to extract

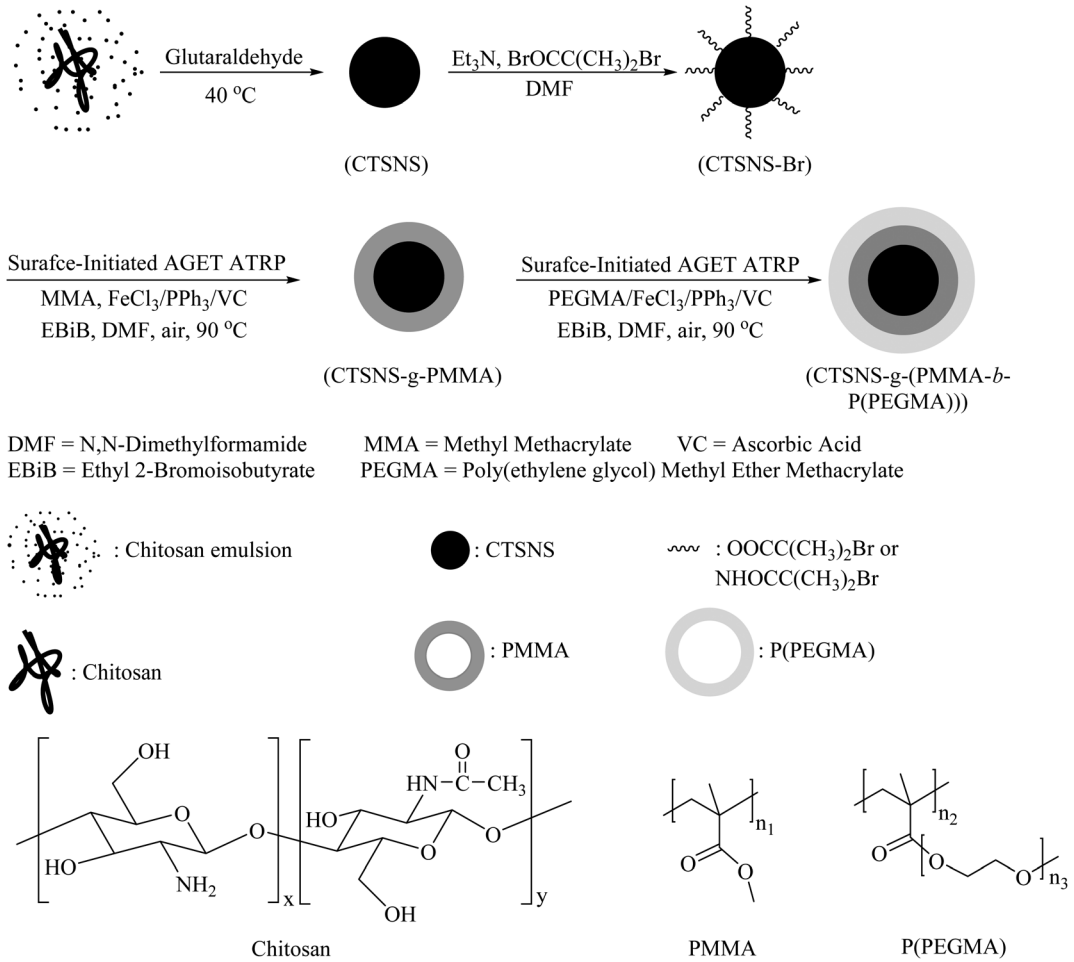

Fig. 10 Surface modification of chitosan nanospheres (CTSNS) by ATRP for the synthesis of CTSNS-Br, CTSNS-*g*-PMMA, and CTSNS-*g*-(PMMA-*b*-P(PEGMA)). Adapted from ref. 114. Copyright 2014, with permission from ACS.

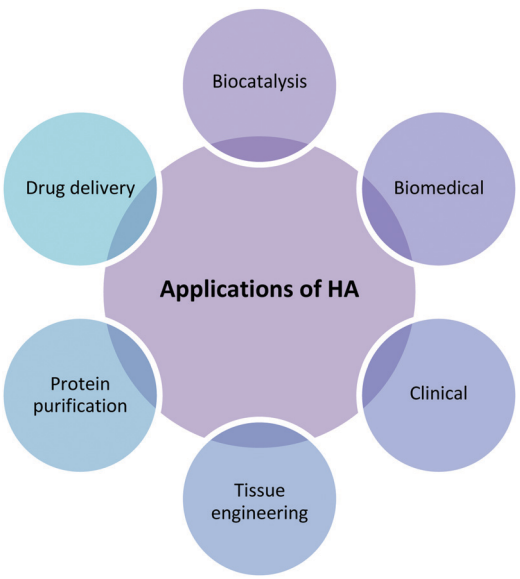

Fig. 11 Major applications of HA.

natural hydroxyapatite (bio-HA). Consistent with the aim of this review, relevance is given here mostly to properties and applications of bio-HA. Extraction methods of bio-HA have been described starting from many different natural residues including animal bones, fish scales, eggshells, seashells and algae.[121] The treatment of animal bones either from bovine, swine or fish sources generally requires removal of residual proteins through alkaline washing followed by high temperature calcination in the 600–1400 °C range. In a comparative study, three protocols such as thermal decomposition and subcritical water and alkaline hydrothermal processes were explored for the isolation of natural hydroxyapatite from bovine bones.[122] All methods afforded similar yields of bio-HA (~65%): the thermal process (750 °C, 6 h) provided nanorod shaped HA of about 300 nm, while both alkaline hydrothermal process (NaOH, 25 wt%; 250 °C, 5 h) and treatment in subcritical water (275 °C, 1 h) gave pure hydroxyapatite nanoparticles of smaller size (<100 nm). In particular, subcritical water produced HA nanoflakes by plucking out residual collagen from bones.

Mild procedures were reported starting from fish scale (FS) waste for which simple deproteinization was carried out with HCl (0.1–1 M, r.t.), NaOH (5–50 wt%, 70–100 °C), and/or heating

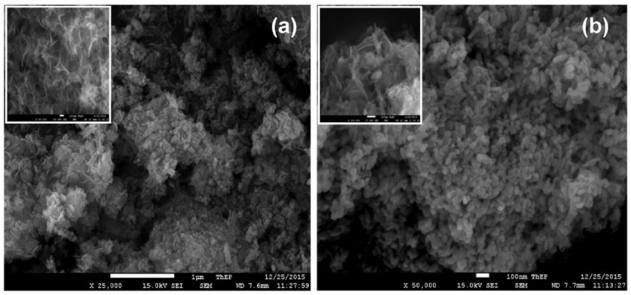

Fig. 12 SEM images of bio-HA extracted from the fish scales of golden carp (left) and synthetic HA (right). Adapted from ref. 124. Copyright 2016, with permission from Elsevier.

in boiling water, without any calcination at high temperature.[123,124] In a first example, bio-HA extracted from FS of *Tilapia nilotica* proved 4-fold more efficient than commercial hydroxyapatite for the selective adsorption and removal of Se(IV) in the purification of drinking water.[123] Even more remarkable were the properties of HA obtained from the FS of golden carp (*Probarbus jullieni*): with respect to synthetic HA, bio-HA improved the formation of apatite during incubation in simulated body fluid, and it showed higher osteoblast like cell adhesion on its surface, thereby proving its potential as a bioactive material for bone scaffolds and tissue regeneration.[124] This behaviour was correlated to the results of SEM, TEM, and EDX analyses showing that the bio-derived hydroxyapatite had a larger surface area, was richer in Ca, and had higher surface roughness than synthetic HA, and it was composed of rod-shaped (50 nm in diameter) and flat-plate (*ca.* 20 × 100 nm, width × length) nanocrystals, respectively (Fig. 12).

It should be noted here that sHA is a stoichiometric solid with a Ca/P ratio of 1.67, while the bio-HA from biowaste is not, due to the presence of trace amounts of cations and anions such as Mg^{2+}, Na^{+}, K^{+}, Zn^{2+}, Sr^{2+}, Al^{3+}, Cl^{-}, F^{-}, CO_3^{2-} and SO_4^{2-}. This feature was reported to impart further beneficial properties to bio-HA especially for the rapid regeneration of bone tissue.[121,125] In this respect, *in vitro* studies compared the biological response of sHA and three natural HAs extracted from fish bones of rainbow trout, cod and salmon, respectively, proving that bio-HA from trout and salmon showed a higher activity towards osteoblasts (MC3T3-E1) than the other tested materials. The result was ascribed to the effect of both CO_3^{2-} and Mg^{2+} ions (~0.7 wt%) able to stimulate cell proliferation, adhesion, differentiation, and mineralized tissue formation.[126] A related concept was applied in the fabrication of a nanocomposite scaffold of natural hydroxyapatite and chitosan extracted from bovine cortical bone and shrimp shells, respectively, containing iron oxide nanoparticles of 10–40 nm.[127] This combination afforded a super-paramagnetic material with a saturated magnetic intensity of approximately 3.04 emu g^{-1} and a coercive force of 128.39 Oe, potentially suitable for bone healing therapies. Another interesting biocomposite was devised by the electrochemical deposition of a coating of chitosan, silver, and hydroxyapatite on anodized titanium substrates.[119] Although synthetic HA was used in this case, the synergistic effect of the antibacterial properties of chitosan and silver ions and biocompatibility of HA with bone tissue provided a coating preventing the risk of bacterial infection of implants.

$$CaCO_3 \xrightarrow{\text{calcination}} CaO + CO_2$$

$$3\,Ca_3(PO_4)_2 + CaO + H_2O \longrightarrow Ca_{10}(PO_4)_6(OH)_2 \quad (a)$$

$$10\,CaO + K_2HPO_4 + 4H_2O \longrightarrow Ca_{10}(PO_4)_6(OH)_2 + 12\,KOH \quad (b)$$

Scheme 1 Preparation of s-HA from CaO and two phosphorus salts (a and b).

Biowastes such as eggshells and seashells have been also reported as a source for the preparation of HA.[121,128] In this case however, the shell residues are calcined to obtain CaO which in turn is converted to HA by reaction with phosphorus salts (Scheme 1). The final HA product is therefore a synthetic material.

There are several reports on the preparation of different HA-based catalysts and their catalytic applications in chemical reactions.[129] Different applications of HA-based catalysts have been summarized in Table 2.

2.4 Bioplastics

Bioplastics encompass both bio-based materials synthesized from biomass and bio-degradable plastics which break down into organic matter and gases, mostly CO_2, by the action of naturally occurring microorganisms including algae, fungi, and bacteria. The latter may be of fossil or renewable origin.[170] Plastics can thus be categorized into four groups given their biodegradability and raw materials (Fig. 13).[171]

Examples of well-known non-biodegradable and biodegradable oil-based plastics include polyethylene (PE), polypropylene (PP), and poly(ethylene terephthalate) (PET) in the first group (non-biodeg.), and poly(e-caprolactone) (PCL), poly(butylene succinate/adipate) (PBS/A), and poly(butylene adipate-*co*-terephthalate) (PBA/T) in the second family, respectively.

On the other hand, not all bio-based plastics are necessarily biodegradable: in contrast to cellulose, cellulose acetate does not decompose in the environment. Likewise, bio-PET from bio-based ethylene glycol, whose content of renewable C is approximately 30%, is not a biodegradable polymer.

European Bioplastics has estimated that the worldwide production capacity for bioplastics is set to increase from *ca.* 2.05 million tonnes in 2017 to almost 2.44 million tonnes in 2022, with fully bio-based and biodegradable biopolymers such as PLA (polylactic acid) and PHAs (polyhydroxyalkanoates) as the main drivers of this growth (Fig. 14).[172] However, non-biodegradable polymers sourced from biomass such as bio-PE (polyethylene) and bio-PET (polyethylene terephthalate), which presently constitute *ca.* 56% (1.2 million tonnes) of the worldwide bioplastics production, will follow different fates. The manufacture of bio-based PE is predicted to continue growing in the coming years, while that of bio-based PET will not at the expense of a new 100% bio-based substitute such as bio-PEF (polyethylene furanoate), with improved barrier and thermal properties for the packaging of drinks, food and non-food products.

Table 2 Summary of different types of HA-based catalyst applications in chemical reactions

Entry	Catalyst	Application	Ref.
1	PdHAP-1	Mizoroki–Heck and Suzuki–Miyaura coupling reactions	130
2	Pd/HAP	Suzuki–Miyaura coupling reaction	131
3	PdFAP[a]	Suzuki–Miyaura coupling reaction	132
4	HAP	Knoevenagel condensation	133
5	Ionic liquid functionalized HAP-γ-Fe_2O_3	Knoevenagel condensation	134
6	Porous calcium HAP	Knoevenagel condensation	135
7	Cobalt HAP	Knoevenagel condensation	136
8	HAP, $NaNO_3$/HAP and $NaNO_3$/HAP/BTEAC[b]	Claisen–Schmidt condensation	137
9	HAP	Michael addition of mercaptans to chalcone compounds	138
10	HAP and NaHAP	Michael-type addition of amines to α,β-unsaturated carbonyl compounds	139
11	ZnHAP	Michael addition of indoles with electron-deficient olefins	140
12	PdHAP-0	Oxidation of alcohols using O_2	141
13	RuHAP	Oxidation of alcohols using O_2	142
14	RuHAP-γ-Fe_2O_3	Oxidation of alcohols using O_2	143
15	RuHAP	Oxidation of silanes	144
16	AuHAP nanoparticles	Oxidation of silanes	145
17	Au nanoclusters/HAP	Styrene epoxidation and aerobic oxidation of benzyl alcohol	146
18	HAP	Epoxidation cyclohexene using H_2O_2	147
19	HAP/TiO_2	Photodegradation of MB	148
20	Pd-TiO_2-HAP nanoparticles	Photocatalytic oxidation of potassium cyanide	149
21	HAP/TiO_2 nanocomposite	Photocatalytic oxidation of nitrogen monoxide	150
22	Fe_3O_4/HAP nanoparticles	Photodegradation of diazinon	151
23	Pd/HAP/Fe_3O_4	Photocatalytic degradation of azo dyes	152
24	HAP	Photocatalytic decomposition of methyl mercaptane	153
25	Pt/ZnO/HAP	Photocatalytic oxidation decomposition of benzene	154
26	$SbCl_3$-HAP	Preparation of *trans*-pyrano[3,2-*c*]quinolones	155
27	HAP, $ZnCl_2$/HAP, $NiCl_2$/HAP and $CuCl_2$/HAP	Friedel–Crafts alkylation	156
28	AgHAP nanoparticles	Hydration of nitriles	157
29	HAP and $ZnCl_2$/HAP	Transesterification reaction	158
30	HAP supported rhodium	Hydroformylation of 1-hexene	159
31	Pd(0)HAP	Hydrogenolysis of 4-chlorphenol	160
32	RuHAP	Hydrogenation of levulinic acid	161
33	RhHAP	Hydrogenation of nitroarenes with hydrazine	162
34	Au nanoclusters/HAP	Hydrogenation of nitrobenzene and oxidation of styrene	163
35	Ru-HAP	Hydrogenation of various renewable oils	164
36	Pd–Co/HAP	CO-cleanup of H_2-rich stream	165
37	Ni/HAP	Propanol amination	166
38	Au/γ-Fe_2O_3@HAP	Reduction of 4-nitrophenolate to 4-aminophenolate	167
39	Pd_3/HAP	Conversion of glycerol to lactic acid	168
40	HAp	Ketose production	169

[a] FAP: fluorapatite. [b] Benzyltriethylammonium chloride.

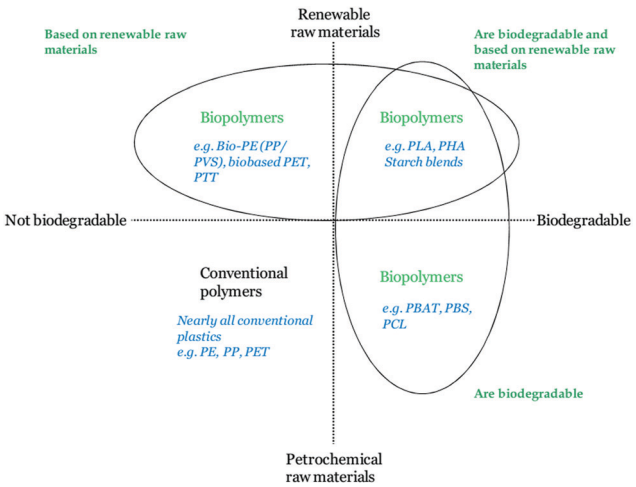

Fig. 13 The four general types of plastics grouped by materials of renewable (top) and fossil (bottom) origin, not biodegradable (left) and biodegradable (right) polymers, respectively.[171]

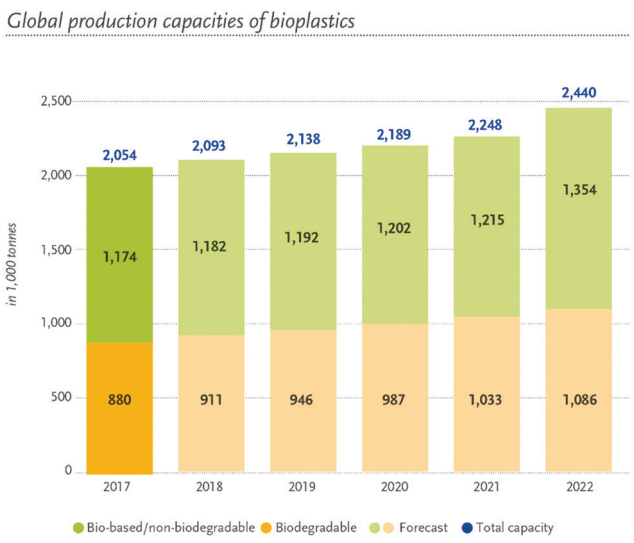

Fig. 14 Trend in the global production of bioplastics.[172]

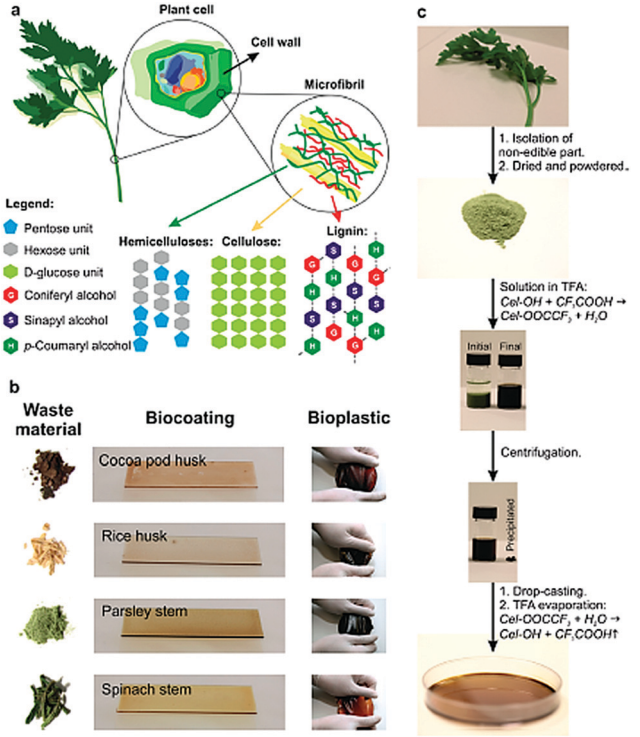

Fig. 15 Edible plant waste products. (a) Schematic of the main components (hemicellulose, cellulose and lignin) of inedible plant wastes and their distribution at different scales. (b) Different edible plant wastes in diverse forms used in this study. Also, the resultant biocoating and bioplastic products are shown. (c) Bioplastic production process from plant wastes to final films. Pulverized vegetable waste is dissolved in TFA and after an appropriate aging time is reached the solution is cast into a Petri dish. Centrifugation can be used in order to eliminate undissolved parts. Adapted from ref. 175. Copyright 2014, with permission from ACS.

Due to the vast proportions and complexity of this subject, the present review paper will limit the analysis only to selected examples aimed at enabling the Reader to get a perspective on innovative studies in the field of bioplastics prepared from secondary feedstocks as biowastes.[173]

A recent investigation has proposed the use of myofibrillar proteins from residues of the processing of gilded catfish (*Brachyplatystoma rousseauxii*) to synthesize new plastic materials. Once extracted, proteins were mixed with aq. glycerol as a plasticizer, and by a casting method, the resulting solutions were added to a silicone support and dried to get biofilms.[174] A response surface methodology was employed to optimize the process design, obtaining a bioplastic with 40% plasticizer (m/m) and 0.79% protein (m/v). The protein content imparted flexibility, resistance, low solubility and water vapor permeability which made the material suitable for food packaging. The good tensile strength (4.91 MPa) was ascribed to the extent of sulfhydryl groups at the myofibrillar protein surface which enabled the formation of covalent S–S in the biofilm framework. On the other hand, the hydrophilicity of fish muscle proteins due to their content of polar amino acids and hydroxyl (OH) groups was responsible for the low moisture barrier (water vapor permeability, WVP, in the range of 6–14 g m^{-1} s^{-1} Pa^{-1}) of the bioplastic.

A method for digesting edible vegetable waste (rice hulls, cocoa pod husks, wastes of parsley and spinach stems) with trifluoroacetic acid (TFA) was explored to prepare amorphous cellulose-based plastics.[175] Dehydrated residues (3 wt%) were dispersed in TFA for variable periods (3–14 days) until dissolution; thereafter, casting processing and solvent removal under controlled humidity (60%) afforded biofilms (Fig. 15). Interactions of TFA with the cellulose component of the wastes brought about either breaking of the hydrogen bonds between neighboring cellulose chains (intersheet hydrogen bonds), or partial trifluoroacetylation of OH groups of cellulose with formation of amorphous materials. The mechanical properties of biofilms were largely dependent on the starting biowaste: residual silica in the rice hull derived material conferred rigidity, while the triglyceride content in cocoa pod husks was responsible for the high stresses at break and strains of the corresponding film. This behavior along with the assessment of other properties (Young's modulus and interaction with water) compared with common polymers (polypropylene, polyethylene, polyester) and elastomers (silicone and polyurethanes) indicated that vegetable waste bioplastics could open avenues for task-specific applications in packaging and biomedicine.

The color of the resultant bioplastics from plant wastes is brown (Fig. 15).[175] Generally, similar colours were observed for most generated bioplastics from vegetable and cereal waste feedstocks, in certain cases requiring blending or pre/post-treatments to reach transparency.

With the further progress of this investigation, micronized powders of vegetable waste from carrots, radicchio, parsley and cauliflower were dispersed in conc. HCl (50 mg solid per mL) at 40 °C for 12 hours. Viscous dispersions were then dialyzed on a 3500 Da membrane against pure water and cast/dried to get the corresponding biofilms.[176] Confocal microscopy and SEM analyses proved the formation of homocomposites with particle sizes of 1–100 μm for carrots, parsley and cauliflower or larger for radicchio, displaying higher stiffness and lower ductility (Young's modulus and ultimate strength in the range of 0.2–1.3 GPa and 3–38 MPa, respectively) than bioplastics reported in Fig. 15. Solid-state NMR characterization further showed that films were comprised of cellulose crystals fused together, with pectin and sugar portions acting as plasticizers. Notably, a blend polymer of polyvinyl alcohol (PVA) and carrot bioplastic showed an oxygen permeability (OP) of 31.2 cm^3 μm m^{-2} day^{-1} kPa^{-1}, lower than that of synthetic films, and migration of its components to food (tested against the dry food simulant Tenax®) well below 10 mg dm^{-2} which is the threshold value in EU for materials used in food contact. Similar low values of release to food, in the range of 1.2–3.5 mg dm^{-2}, were noticed also for bioplastic films as such. Overall, the new class of fully biodegradable compounds could be used for packaging or blended with other polymers for application as disposable objects, cosmetics and biodegradable electronics.

Another frontier in this field is the preparation of biowaste-derived biodegradable plasticizers able to reduce brittleness, crystallinity, glass transition temperature and melting temperature, and improve flexibility and toughness of bioplastics.[177] Fully renewable plasticizers have been described for both

poly(lactic acid) and poly-3-hydroxybutyric acid (PHB). Significant examples are ethyl citrate synthesized by the esterification with bioethanol of citric acid (2-hydroxy-1,2,3-propanetricarboxylic acid) extracted from orange waste,[178] and tannic acid [1,2,3,4,6-penta-*O*-{3,4-dihydroxy-5-[(3,4,5-trihydroxy benzoyl)oxy]benzoyl}-D-glucopyranose] from residual lignocellulosic biomass.[179] It should be mentioned here that the use of bio-plasticizers is continuously expanding also for the replacement of conventional compounds in synthetic plastics. To cite only two cases, diesters of isosorbide, a common derivative of glucose, and highly branched polycaprolactone prepared by solvent-free copolymerization of ε-caprolactone and glycidol (a derivative of glycerol) have been recently proposed as effective plasticizers of PVC, one of the most valuable polymers worldwide.[180,181] These bio-based plasticizers were claimed to improve the thermal stability and stretchability (~20-fold higher) of PVC with respect to classical petro-based compounds such as phthalate esters.

2.5 Silica and silicates

Biowastes are becoming increasingly interesting for the preparation of both silica and silicate salts.

Silica. In the chemosphere, plants start the biogeochemical cycle of silicon with the uptake of silicic acid (H_4SiO_4) present in soil water. Silicic acid then undergoes polymerization and hydrated amorphous silica forms and accumulates in phytoliths that confer rigidity to plants.[182] Hydrated amorphous silica is naturally occurring in leaves, husks, blades, hulls, roots and stems of many terrestrial and marine plants, including wheat, rice, horsetails, oats, barley, grasses, and algae.[183] Among biowastes, one of the most silica-rich sources is rice husks (RHs) which are largely available, being typically 20–22 wt% of rice grains. The silica content amounts to *ca.* 20% of RHs' dry weight which means that at the current rate of estimated global rice production of 500 Mt year^{-1}, applications of bio-silica and its derivatives are becoming attractive.[184,185] Approaches for the extraction of biogenic silica from RHs are mostly based on acidic pre-treatments for the removal of trace amounts of metals, followed by pyrolytic procedures carried out at variable temperatures and times usually in the range of 500–700 °C and 8–24 hours, respectively.[186] The conditions and process parameters (T and t) could be tailored to afford the synthesis of different added-value meso/macroporous silica. In this respect, one example described the pyrolysis of HCl-treated RHs at 700 °C for 2 h for the preparation of amorphous silica nanoparticles with a narrow size distribution of 25–30 nm (Fig. 16, left).[185] The so-obtained biogenic material was then suspended in aq. KNO_3 and subjected to a second pyrolytic cycle (800 °C, 2–8 h) to achieve a semicrystalline porous silica framework (Fig. 16, right).

As the pyrolysis was prolonged, K^+ cations progressively penetrated the silica structure thereby favoring the fusion of nanoparticles into a new well-defined porous material.

Another remarkable application of biogenic silica has been reported for the fabrication of nanomaterials used in lithium ion batteries. This subject was extensively reviewed in a recent paper describing protocols for the reduction of RH-derived SiO_2 as such or in a blend with carbon to obtain anodes of silicon or silicon/carbon (Si/C) composites and silicon carbide (SiC) materials, respectively.[187] Carbothermal reactions in an electric arc furnace at 1700–2100 °C, and magnesio- and calcio-thermic reactions carried out with biogenic SiO_2 in the presence of powdered Mg and Ca, respectively, at 650–720 °C, were used to prepare high purity silicon (99.9%). The potential of these procedures was discussed as a sustainable alternative for the conventional blast-furnace production of metallurgical-grade (MG) silicon by the reduction of quartz with charcoal at $T > 1900$ °C.

A further contribution in this field proposed the extraction of SiO_2 from eco-friendly and inexpensive agricultural residues such as rice husk (RH), sugarcane bagasse (SB) and bamboo culm (BC) using microwave assisted solid state ashing (MW-SS: 2.45 GHz; 650 °C for 30 min at 1200 W).[188] In the same work, biogenic amorphous silica was subjected to MW-mediated magnesiothermic reduction to prepare crystalline pristine Si that, in contrast to commercial Si nanopowders, displayed a coherent interconnected 3D porous structure with a pore diameter of 50–80 nm and a wall thickness of ~23 nm (Fig. 17, top).

Crystalline Si derived from biogenic silica was finally decorated with dimensionally modulated carbon-based materials such as carbon (C), graphene nanosheets (GNS), and multiwall carbon

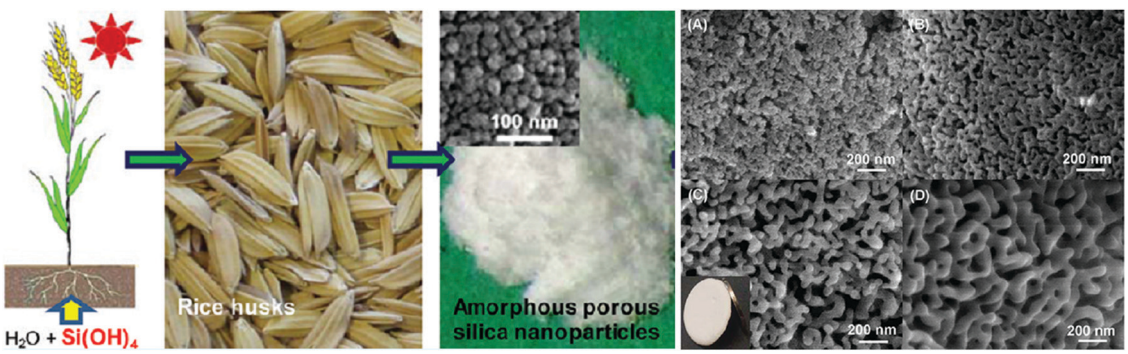

Fig. 16 Left: Amorphous silica from rice husks. Right: Modification of amorphous silica by aq. KNO_3. SEM images of meso/microporous silica frameworks: (A) 0.20 M KNO_3, pyrolysis at 800 °C for 2 h; (B) 0.20 M KNO_3, pyrolysis at 800 °C for 4 h; (C) 0.20 M KNO_3, pyrolysis at 800 °C for 8 h; (D) 0.50 M KNO_3, pyrolysis at 800 °C for 8 h. The inset in (C) shows a coin shaped disk made of the corresponding semicrystalline porous silica framework. Adapted from ref. 185. Copyright 2012, with permission from ACS.

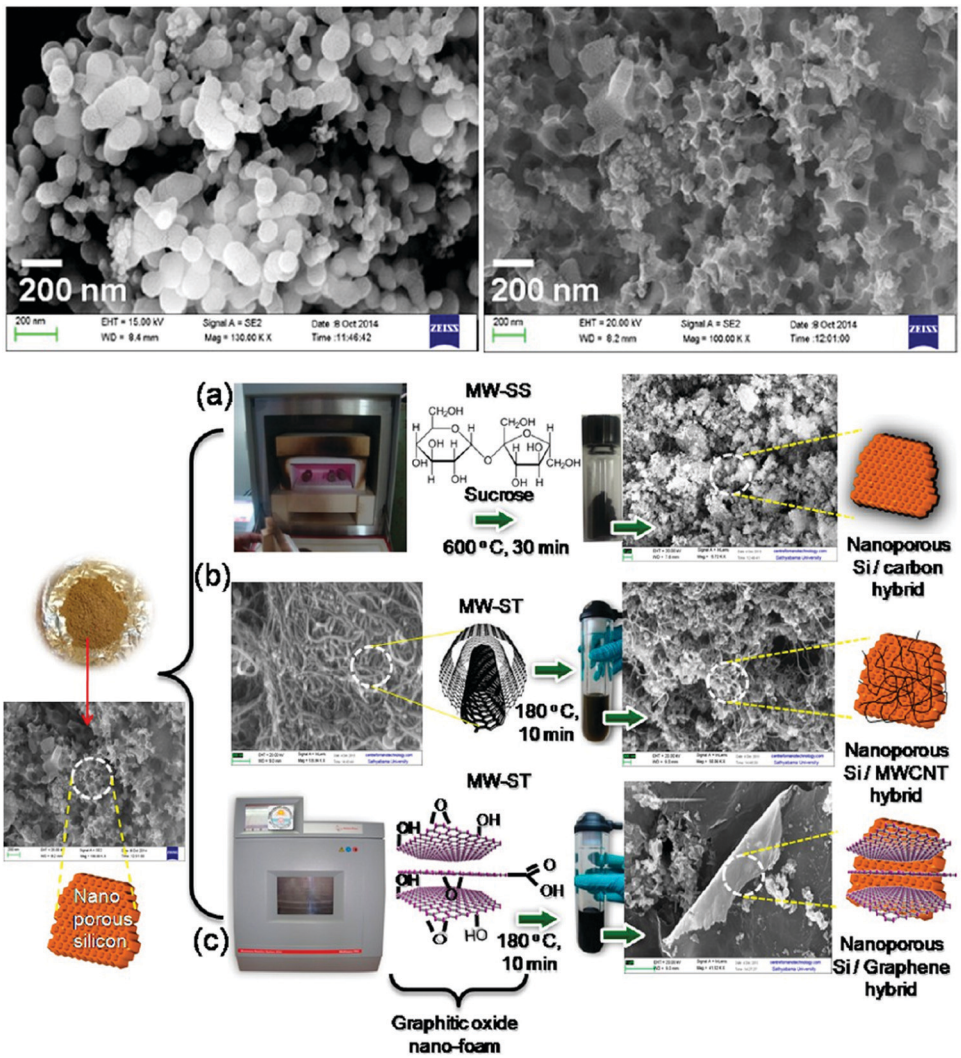

Fig. 17 Top: Comparative FESEM images of commercially available agglomerated Si (left) and nanoporous Si obtained from biogenic silica *via* microwave assisted magnesiothermic reduction (MW-MR) within 30 min at 650 °C (right). Bottom: Silicon-based nanohybrid prepared by (a) microwave assisted solid state (MW-SS) decoration of carbon on 3D nanoporous silicon at 600 °C within 30 min, (b) microwave assisted solvothermal (MW-ST) synthesis of silicon and MWCNT nanonetworking at 180 °C in 10 min, and (c) *in situ* one-pot MW-ST synthesis of 3D nanoporous silicon decorated on graphene nanosheets (GNS) at 180 °C in 10 min. Adapted from ref. 188. Copyright 2015, with permission from ACS.

nanotubes (MWCNT) (Fig. 17, bottom). These materials offered delithiation capacities of 1997, 1290, and 1166 mA h g^{-1}, respectively, higher than pristine Si (956 mA h g^{-1}) from RHs, and interesting for next generation anodes in lithium batteries.

Silicates. Biogenic silicates can be obtained from biowastes *via* two general avenues including the chemical extraction of rice husks or the use of inorganic biowastes, mostly egg or oyster shells, as a source of Ca to provide the corresponding silicate salts.

Starting from RH ash, chemical methods are generally based on alkaline extraction with aq. NaOH (1–3 M) under both conventional and microwave-induced heating.[186,187] Under these conditions, the silica contained in ash is dissolved forming sodium silicate which is then neutralized to precipitate silica gels (Scheme 2).

Starting from eggshells, recently a sol–gel combustion method was developed by first dissolving shell waste in nitric acid, and then adding magnesium nitrate, citric acid and TEOS (tetraethyl orthosilicate). Nitric acid served both to control the

$$SiO_2 + 2\,NaOH \longrightarrow Na_2SiO_3 + H_2O$$
(ash)

$$Na_2SiO_3 + HX \longrightarrow SiO_2 + NaX + H_2O$$
Silica gel

X = Cl, NO_3

Scheme 2 Chemical treatment of RH ash.

pH (= 1) of the reaction mixture and to facilitate the hydrolysis of TEOS into silanol and ethyl alcohol. After 28 h at r.t., polycondensation of silanol and ethyl alcohol with citric acid provided a gel-like product which was finally decomposed in a muffle furnace at 400 °C. The synthesis yielded a nanocrystalline calcium magnesium silicate (akermanite, $Ca_2MgSi_2O_7$) with particle size in the range of 80–90 nm. *In vitro* bioactivity tests of this material in simulated body fluid proved the formation of a crystallized hydroxyapatite layer on its surface, thereby disclosing its potential for application in hard tissue regeneration.[189]

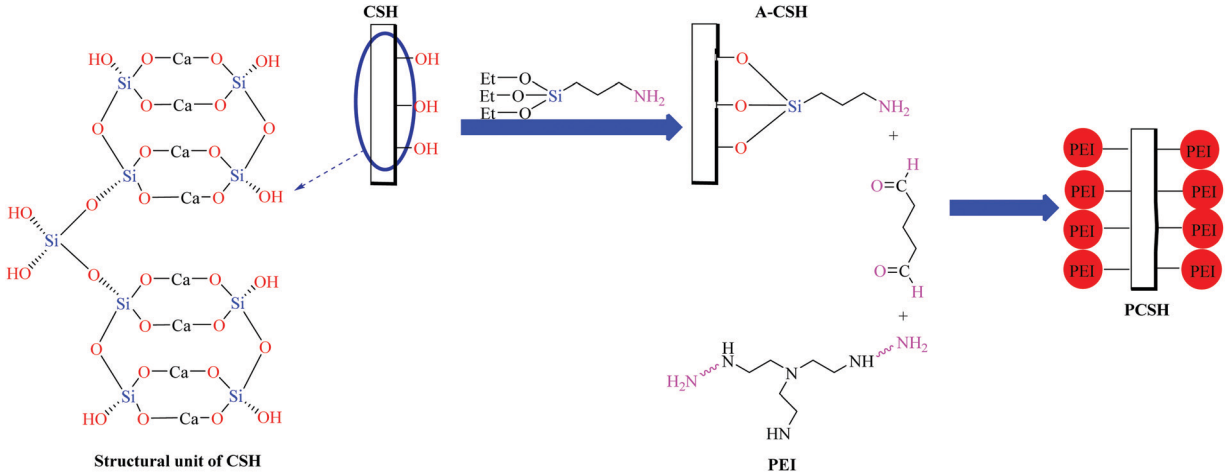

Fig. 18 Preparation of PEI-functionalized calcium silicate hydrates (PCSH). Adapted from ref. 190. Copyright 2016, with permission from the Royal Society of Chemistry.

The synthesis of excellent adsorbents for environmental metal remediation was conceived starting from oyster shells (OS), an abundant biowaste product from mariculture. Calcium silicate hydrates (CSH) were first prepared through the calcination of OS in the presence of fumed silica at 650 °C for 2 h, followed by a hydrothermal treatment at 150 °C for 12 h. EDS, SEM and TEM analysis proved that CSH were a mixture of calcium carbonate and calcium silicate hydrates with a hierarchical porous structure with a large surface area composed of thin nano-sheets each of which was assembled by nanofibers with width and length of about ten and hundreds of nanometers, respectively. The surface of CSH was then modified by a multistep sequence including the functionalization with 3-aminopropyltriethoxysilane and further reactions with glutaraldehyde and polyethyleneimine (PEI) (Fig. 18).[190]

The grafting of PEI did not modify the size and morphology of the final material (PCSH) with respect to CSH; however, the high density of surface amino groups able to chelate metal cations strongly improved the adsorption capacity of PCSH up to 256 and 203 mg g^{-1} for aq. Cr(VI) and Cu(II), respectively. This (capacity) was much higher than that of OS, CSH and many other adsorbents reported in the literature.

2.6 Additional miscellaneous examples

Besides the examples detailed in the above paragraphs of Section 2, several other studies on the fabrication of biomaterials derived from biowastes have been described in the literature of the past fifteen years. Table 3 provides a summary of additional relevant examples.

Table 3 Biomaterials derived from biowastes

Entry	Biowaste	Prepared biomaterials	Ref.	Entry	Biowaste	Prepared biomaterials	Ref.
1	Bovine bones	Mineralized collagen	191	2	Fish waste	Gelatin	192
3	Silver carp skin	Collagen	193	4	Fish fin and chicken feather waste	Protein	194
5	Mantis shrimp muscle	Collagen	195	6	Fish bone	Calcium phosphates	196
7	Puffer fish skin	Collagen	197	8	Groundnut and coconut shell, rice husk, palm fruit bunch and palm fruit stalk	Cellulosic fibers	198
9	Cuttlefish skin	Collagen	199	10	Pig bones and teeth	Hydroxyapatite	200
11	Brown backed toadfish skin	Collagen	201	12	Eggshells	Nanostructured hydroxyapatite	202
13	Fish (*Lates calcarifer*) scales	Collagen sheet	203	14	Eggshells	Mesoporous hydroxyapatite NPs	204
15	*Loligo uyii* skin	Type V collagen	205	16	Fish scales	Hydroxyapatite scaffolds	206
17	Eel fish skin	Type-I collagen	207	18	Shrimp shells	Bioplastic	208
19	Milkfish scales	Collagen	209	20	Chicken feathers	Bioplastic	210
21	Prawn shells	Chitosan	211	22	Fish scales	Bioplastics	212
23	*R. oryzae* fungi on potato peels	Chitosan	213	24	Rice husk	Polyester bioplastic	214
25	Goatskin	Collagen–chitosan biocomposites	215	26	Food industry	Bioplastic	216
27	Fish (*Labeo rohita*) scales	Chitin and chitosan	217	28	Fruit peel	Bioplastic	218
29	Shellfish	Chitosanases	219	30	Wood mill effluents	Bioplastic	220
31	Crustacean	Chitin	221	32	Rice husk	Porous SiO_2	222
33	Blue crab	Chitosan	223	34	Rice husk	Nanosilica	224
35	Crab shells	Chitin and chitosan	225	36	Rice and coffee husks	Cellulose nanocrystals	226
37	Shrimp shells	Chitosan and chitooligosaccharides	227	38	Cotton linters and kraft pulp	Cellulose nanocrystals	228
39	Beetle (*Catharsius molossus*)	Chitosan	229	40	Croaker fish skin	Gelatin	230

3. C-Based and hybrid C-based nanomaterials

3.1 Nano-carbons and nanocomposites

The nanocarbon family encompasses sp^2-bonded carbon materials with a variety of morphologies, including fullerenes, nanotubes and nanoscrolls, 2D-honeycomb arranged graphene, nanodiamonds and activated carbon nanoparticles and fibers (Fig. 19, left).[231,232] Nanocarbons combine the unique properties of high mechanical flexibility (in the case of graphene and carbon nanotubes), stability, ultra-high surface area, low toxicity, biocompatibility and tunable electrical, chemical and physical properties by covalent and non-covalent functionalization, which have contributed to make them increasingly popular as new materials for (i) fillers in composites and hybrids, (ii) chemical- and bio-sensing in medicine, (iii) energy electrocatalysis and energy storing in the fabrication of supercapacitor electrodes, (iv) bioelectronics platforms, (v) enhanced supports for precious metal-based catalysts, (vi) plant growth promoters, *etc.* (Fig. 19, right).[233–236]

In recent times, the interest in nanocarbons has further expanded owing to the implementation of sustainable synthetic routes starting from biowastes.[237] Collagen turned out to be a promising source, particularly that derived from leftovers of the leather industry. One of the first waste-to-wealth approaches was described using waste goat skin trimming from which collagen was extracted and then treated by heating in a flow of Ar at 500–1000 °C.[238] Onion-like C-based structures, measuring up to ~20 nm, were obtained, each of them consisting of an assembly of defective spherical shells of graphite like layers separated from each other by approximately 3.36 Å. XPS and elemental analyses proved that the graphitic layers were doped by O- (6–15%) and N-atoms (3–15%) in the form of C=O and –O–C(O)O– groups, and N-bearing aromatic rings, respectively. These materials, particularly those obtained at 1000 °C, displayed an electrical conductivity of 4.6×10^{-1} S m^{-1} comparable to that of pristine graphene powder. In a second example, collagen extracted from raw cowhide trimming waste was added to aq. AcOH and superparamagnetic iron oxide nanoparticles (SPION). After gentle heating (40 °C, 12 h) and freeze-drying (4 °C, 18 h), a sponge-like highly porous interconnected material was achieved in which the collagen fibrils were cross-linked with the inorganic nanoparticles (Fig. 20, top).[239]

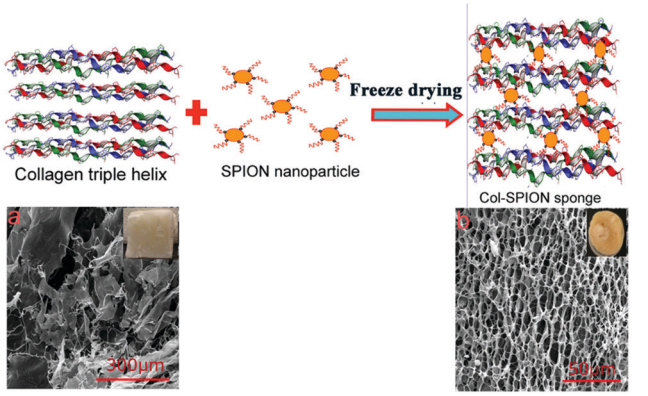

Fig. 20 Top: Pictorial view of a hybrid composite sponge. Bottom: SEM images of (a) pristine collagen sponge and (b) Col-SPION hybrid sponge. Adapted from ref. 239. Copyright 2016, with permission from ACS.

Characterization of the composite proved that the collagen triple helical structure was not altered by SPION inclusion into the organic matrix, but strong interactions occurred between the two components of the material explaining its remarkably different 3D morphology with respect to a pristine collagen sponge (Fig. 20, bottom). The structure of the SPION-incorporated collagen sponge was responsible not only for improved mechanical stability, but also for good biocompatibility as demonstrated by the improved proliferation of model cells (293T). The addition of SPION to collagen stabilized its macromolecular structure and significantly improved its cell viability. In fact, the SPION

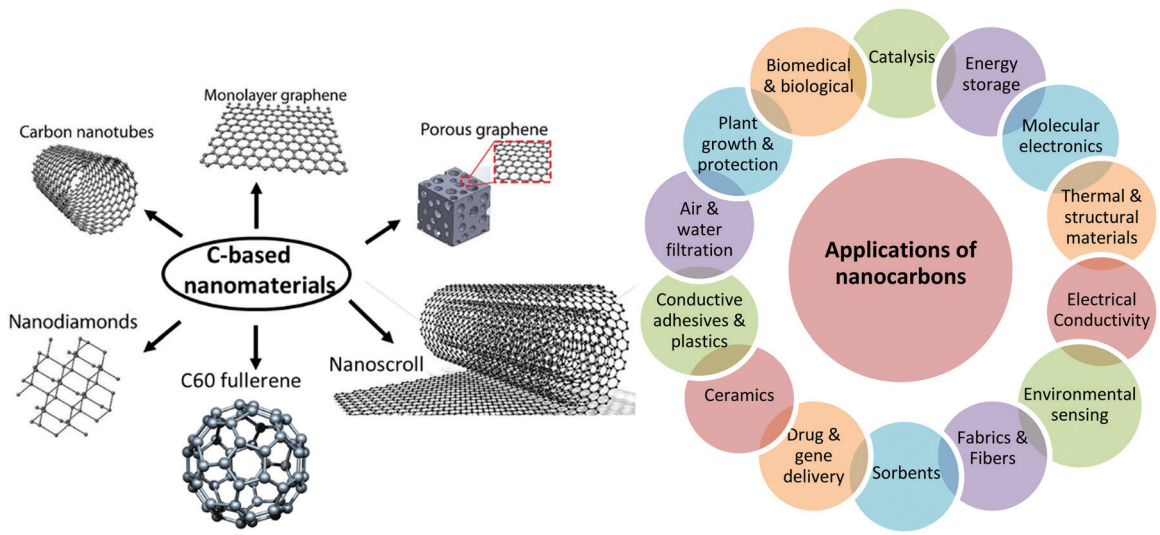

Fig. 19 Left: Examples of C-based nanomaterials; right: application fields of nanocarbons.

incorporated collagen sponge does not inhibit cell proliferation relative to the untreated control cells. According to the literature, 293T cells grow better in the presence of the Col-SPION sponge than in the presence of pristine collagen sponge after 48 h of cell seeding. This was reported to be related to the non-covalent crosslinking between collagen and Fe_3O_4 NPs and the presence of enhanced interconnected porosity, which considerably influenced proliferation, cell attachment and migration.

In a further development of this study, the same type of cowhide trimming waste derived collagen was added to aq. $FeCl_3$, freeze-dried, and finally heated at 1000 °C in an inert atmosphere. A hybrid bi-functional material comprised of iron nanoparticles encapsulated in nanostructured graphitic carbon was fabricated with a surface area over 300 $m^2 g^{-1}$, a conductivity of $3.64 \pm 0.13 \times 10^{-3}$ S cm^{-1}, and a saturation magnetization of 12.3 emu g^{-1}.[240] The adsorption capability of the carbon shell and the separation of electrons and holes by iron nanoparticles made the material an efficient photocatalyst for environmental remediation applications and a potential new system for anodes in Li ion batteries with a reversible capacity of 384 mA h g^{-1}, which is higher than that of graphitic carbon or graphene nanosheets. In this field, another approach was conceived starting from untreated softwood sawdust which was soaked in aq. iron nitrate and carbonized at 800 °C in a muffle furnace under a flow of N_2.[241] Catalytic iron carbide nanoparticles (Fe_3C) were thermally generated *in situ*. These etched through the biomass producing straight and bamboo-like intertwined tubules (diameter of 20–50 nm) with walls composed of graphitic layers similar to multi-walled carbon nanotubes. The same carbothermal reduction was carried out by premixing $Fe(NO_3)_3 \cdot 9H_2O$ with either $Ca(NO_3)_2 \cdot 4H_2O$ or $Mg(NO_3)_2 \cdot 6H_2O$, to prepare nanocomposites of Fe_3C/graphite combined with metal oxide nanoparticles such as MgO or CaO, respectively. All such materials are of interest for a range of technologies including electrocatalysts, battery electrodes and water treatment.

The synthesis of a hybrid material composed of copper sulfide (Cu_2S) carbon nanocomposite was reported starting from an unprecedented method for pig bristles (pb) valorization as a biowaste acting as a source of both C and S. Under microwave irradiation, a mixture of pb, ethylene glycol, and copper chloride underwent a thermo-degradation reaction by which disulfide bonds of keratin, the protein constituting pb, broke down releasing sulphur in the form of ions which in turn combined with Cu^+ and self-aggregated C-particles. The properties of chalcocite (Cu_2S) as a p-type semiconductor (band gap of 1.2 eV) were exploited for the catalytic photodegradation of methyl red, a model for environmentally recalcitrant organic dyes.[242]

Biowaste oil palm leaves (OPL) have been described as another source for the preparation of porous carbon nanoparticles (PCNs), through pyrolytic treatments carried out at 500–700 °C under a N_2 atmosphere.[243,244] Naturally occurring silica in starting leaves acted as a template to provide carbon nanospheres with particle sizes in the range of 20–85 nm. Silica was then removed by alkaline washing (NaOH, 2.5 M, r.t.). Voltammetry studies proved that PCN-based electrodes had a specific capacitance as high as 368 F g^{-1} at 0.06 A g^{-1} in 5 M KOH, indicating that PCNs could be effective precursors for the fabrication of supercapacitor electrodes.

3.2 Carbon dots

Carbon dots, usually abbreviated as CNDs (carbon nanodots) or C-dots, are nano-sized (<10 nm) quasi-spherical carbon particles containing a carbon core functionalized with some of the most common groups, primarily carbonyl and hydroxyl moieties. As such, C-dots are a class of carbonaceous nanomaterials distinct from fullerenes, graphenes, carbon nanotubes, and other carbon allotropes.[245] After their fortuitous discovery in 2004, C-dots have rapidly emerged as a new class of versatile materials able to integrate optical properties of quantum dots based on semiconductors with electronic properties of carbon materials.[246] C-dots have been and are therefore extensively investigated for application in biosensing, bioimaging, drug delivery, photocatalysis, photovoltaic devices, and optoelectronics.

The two most used methods for the preparation of C-dots are the top-down approach in which large macroscale carbon sources are broken down by arc-discharge, laser ablation, and electrochemical reactions, and the bottom-up approach in which thermal, hydrothermal, and microwave-assisted routes allow the assembly of C-dots from molecular precursors. This synthetic flexibility allows one to modify the degree of carbonization, size, and morphology of C-dots, though issues related to batch-to-batch reproducibility, control of surface properties, purification, and characterization may represent a limit for the application of these materials.[247] In this respect, the use of natural products including biowastes as starting materials for the synthesis of C-dots has been reviewed in two recent papers.[248,249] The subject is still in its infancy and there is much room for further discovery, but some original strategies are emerging. For example, hydrothermal-assisted methods have proved effective for a variety of biowastes such as fruit peels, fish scales and rice husks. The heating of an aqueous dispersion of pomelo peel waste at 200 °C for 3 h was reported to produce stable dispersions of C-dots of 2–4 nm, which upon excitation at 365 nm, showed a PL emission peak at 444 nm and an intense blue color under UV light (6.9% quantum yield) (Fig. 21).[250]

Such carbon dots were effective as sensing probes to sensitively detect label free, aq. Hg^{2+} ions with detection limit as low as 0.23 nM. A similar approach was used starting from orange pericarp waste which afforded C-dots with an average particle size of 2.9 nm and PL quantum yield of 2.88%. The narrow size distribution suggested potential applications in nanobiotechnology.[251]

Another method for the synthesis of N-doped photoluminescent C-dots was described using fish scale waste of grass carp that was suspended in deionized water and heated at 200 °C for 24 h in an autoclave.[252] The generated C-dots were homogeneously sized particles of 2 nm with a remarkably high N-content of 14.6% (by XPS) (Fig. 22). A broad emission peak appeared at 430 nm upon excitation at 365 nm with a quantum yield of 17.08% due to the fluorescence enhancement effect of nitrogen doping. The PL effect was strong enough for an aqueous dispersion of C-dots to provide very bright violet-blue luminescence

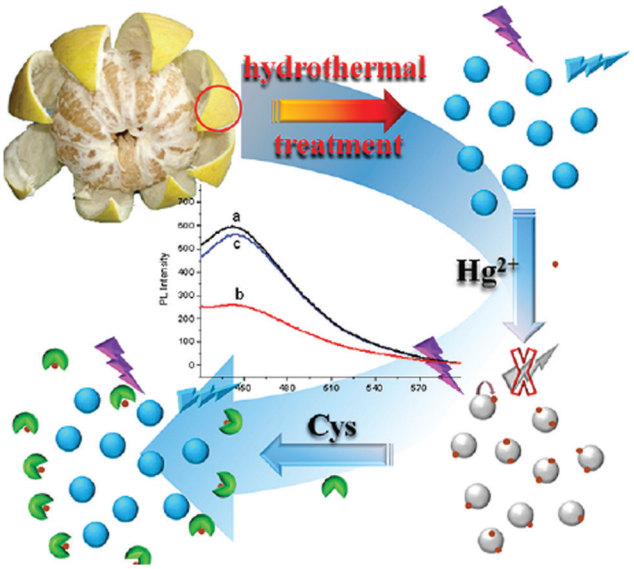

Fig. 21 Hydrothermal treatment of pomelo peel for the preparation of fluorescent CPs sensitive for Hg^{2+} ion detection. Adapted from ref. 250. Copyright 2012, with permission from ACS.

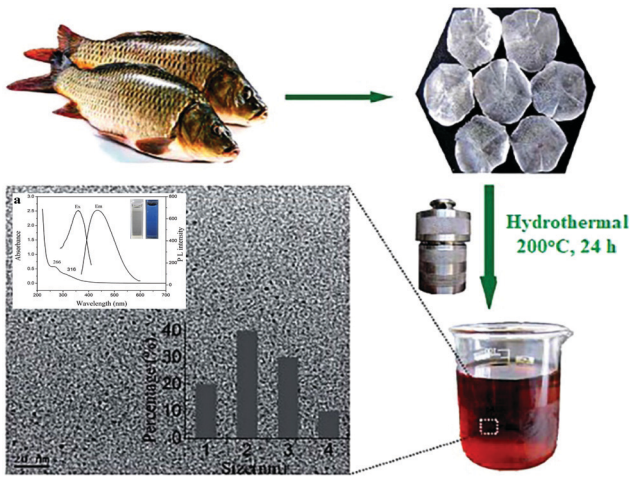

Fig. 22 Schematic illustration of the formation of C-dots from hydrothermal treatment of fish scales. In the TEM image, the insets show the particle size distribution histogram of C-dots (bottom) and their UV-vis absorption, excitation and emission spectra (top). Adapted from ref. 252. Copyright 2015, with permission from the Royal Society of Chemistry.

(top inset of Fig. 22) even at a very low concentration. Notably, the fluorescence could be selectively quenched by ClO^- addition (up to 10 mM), making the fish scale derived C-dots a sensing system for this anionic species.

A multistep "bottom-up" synthesis of C-dots was described starting from rice husks (RHs). The non-oxidative thermal treatment of RHs (700 °C, 2 h) initially generated an ash (RHA) containing both carbon and silica, which was further heated at 900 °C with excess NaOH to produce submicron-sized carbon flakes (RHCs) of 300–500 nm and sodium silicate. The latter was separated *via* aqueous washing and filtration. Solid RHCs were oxidized under acidic/basic conditions and hydrothermally cut at 200 °C, to afford RH-C-dots of 3–6 nm (*ca.* 2 wt% yield based on dry RHs). Aqueous dispersions of such dots were highly stable and showed blue luminescence with emission in the range of 360–440 nm, upon UV excitation at 365 nm. The HeLa cell viability test confirmed that C-dots were biocompatible and useful for cell imaging *via* translocation into the cytoplasm. On the other hand, the recovered sodium silicate was used to synthesize mesoporous silica nanoparticles with a specific surface area and pore diameter of 466 $m^2\ g^{-1}$ and 3.8 nm, respectively. The overall strategy offered an effective approach for a comprehensive utilization of RH biomass.[253]

A microwave-assisted hydrothermal procedure has been also described for the fabrication of C-dots from biowaste, specifically in the treatment of an aqueous mixture of goose feathers, a major discard of the poultry industry, at 180 °C in a microwave autoclave (2 kW). After membrane dialysis (M_w = 3500) against Milli-Q water, an aqueous suspension of C-dots was obtained. C-dots displayed uniform two-dimensional (2D) morphology with a diameter and height of 21.5 and 4.5 nm, respectively, and a content (by XPS) of C, N, S and O of 48.4, 16.3, 1.9, and 33.3 wt%, respectively. Due to heteroatom-doping in the form of surface hydroxyl, carbonyl, carboxylic or amide groups, C-dots showed a high QY of 17.1% upon excitation at 340 nm and acted as selective photoluminescent probes for Fe^{3+} ions with a detection limit of 196 nM.[254]

A different synthetic approach was proposed by using strong acids as oxidants of biomass waste. Starting from dead neem leaves, pyrolysis in a split-tube furnace at 1000 °C (5 h, Ar) provided a fine carbon powder which was added to a 3 : 1 acid mixture of H_2SO_4 and HNO_3 and heated at 90 °C. After filtration (0.2 μm) and neutralization, a stable aqueous dispersion of graphene carbon dots (GC-dots) was prepared. GC-dots were then subjected to a hydrothermal reaction in ammonia solution (30%) at 200 °C for 12 h, to obtain amino-functionalized dots (Am-GC-dots).[255] Some properties and the optical behavior of these materials are summarized in Fig. 23. The surface –COOH functional groups of GC-dots were responsible for the formation of a superlattice due to an extended H-bonding network in which nonradiative recombination of electron–hole pairs was preferred in the intrinsic states. The corresponding green luminescence was attributed to surface energy traps. By contrast, surface $NH_3^+OH^-$ ion pairs led to single monodispersed particles in Am-GC-dots and suppressed the nonradiative path. The observed blue emission was ascribed to zigzag sites.

Overall, Am-GC-dots showed not only much higher water dispersity and photoluminescence intensity than GC-dots, but they also exhibited selective photoluminescence "on–off–on" performance towards aq. Ag^+ ions.

3.3 Three-dimensional porous carbon nano-networks (3DCNT)

3D porous carbon nano-networks identify C-based materials with a peculiar morphology composed of loose three-dimensional network structures possessing a large number of meso- and micropores.[256] Biowastes have been recently proposed as starting materials for the fabrication of such structures. For example, a two-step pyrolytic treatment of goldfish (*Carassius auratus*)

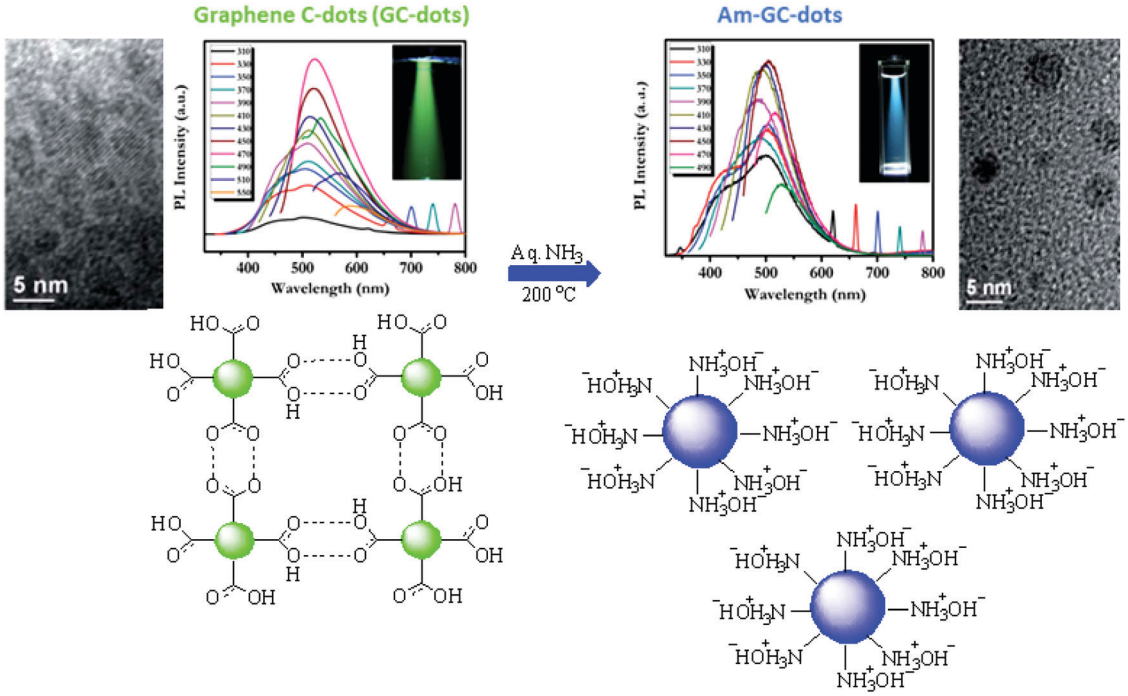

Fig. 23 Top: HRTEM and PL data of GC-dots and Am-GC-dots at different excitations (left and right), respectively; bottom: pictorial views of the GC-dot superlattice due to intermolecular H-bonding and separated Am-GC-dots. Adapted from ref. 255. Copyright 2014, with permission from the Royal Society of Chemistry.

scale waste carried out at 350–900 °C was reported for the synthesis of N-doped hierarchically porous 3DCNT materials.[257] The thermal decomposition took place using $ZnCl_2$ that acted as a promoter for the dehydroxylation of fish scales, thereby increasing the formation of micro/meso-pores within the structure. Moreover, pyridinic- and graphitic-nitrogen dopant species (3–10 wt%) were key components to impart the materials with an electrocatalytic activity for oxygen reduction comparable to that of the commercial 20 wt% Pt/C catalyst in both alkaline and acid solutions (Fig. 24).

In a different approach, a common biowaste such as chicken egg shell membrane (ESM) was used for the preparation of both the electrode material and the bio-separator used in an asymmetric supercapacitor. The protein-rich ESM was firstly carbonized at 800 °C to obtain a 3D carbon network that retained the same fibrous structure of the parent ESM with macropores of 1–10 μm and fibers of diameter of 1–4 μm. Thereafter, the 3DCNT was chemically activated with KOH at 700 °C to form a sheet-like graphitic nanostructure with many surface micropores, which was finally utilized as a support to grow MnO_2 nanoparticles. The asymmetric supercapacitor was then assembled using ESM carbon and MnO_2 nanoparticle/chemical activated ESM carbon as negative and positive electrodes, respectively, and the natural ESM as the separator (Fig. 25). This device displayed a high energy density and power density of 14 W h kg^{-1} and 150 W kg^{-1}, respectively. Significantly, the natural ESM based bio-separator displayed impressive ion conductivity and cycling stability.[258]

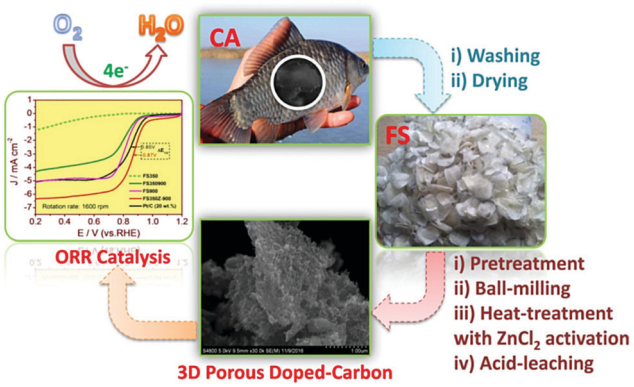

Fig. 24 Preparation of 3D-network nitrogen-doped porous carbon derived from protein-containing FS waste with $ZnCl_2$ activation. Adapted from ref. 257. Copyright 2017, with permission from Elsevier.

Fig. 25 Fabrication of an asymmetric supercapacitor using biowaste-derived materials from chicken egg shells. Adapted from ref. 258. Copyright 2018, with permission from ACS.

In a further development of this study, ground cherry calyces (GCCs) possessing a 3D porous microstructure based on thin-sheets and microtubes were selected as a starting material. The carbonization at 700 °C (4 h, under Ar) of GCCs did not induce a major structural fragmentation. However, the chemical activation/etching of the resulting carbon powder with KOH followed by a further pyrolytic treatment provided a 3D scaffolding framework of porous carbon nanosheets (PCNS) with a typical hierarchical porous structure containing macroporous and mesoporous regions, and co-doped with O and N atoms. SEM analyses are shown in Fig. 26a–c. TEM and XPS proved that the average thickness of the nanosheets was *ca.* 10 nm (Fig. 26d), and the (atomic) contents of C, O, and N of PNCS were ~90.1, ~8.8, and ~1.1%, respectively.

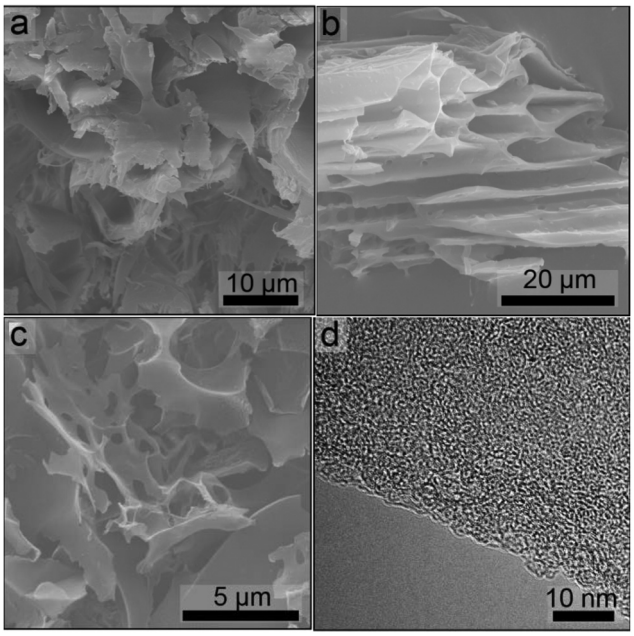

Fig. 26 SEM images of (a) dry GCC; (b) carbonized GCC; (c) PCNS. TEM micrograph of PCNS (d). Adapted from ref. 259. Copyright 2018, with permission from Wiley-VCH.

The combination of meso-, macro- and micropores, the graphitization degree, and the appropriate N,O-doping made this material suitable for fabrication of electrodes for a high-performance supercapacitor displaying a specific capacitance of 350 F g^{-1} at a current density of 0.1 A g^{-1} using 6 M KOH as the electrolyte.[259]

Corncob sponge (CS) was proposed as another biowaste for the preparation of electrode materials. In the reported procedure, CS was mixed with KOH, and activated at 850 °C to obtain a nanocarbon material (ACS) which was doped with N and S by a second pyrolytic treatment (800 °C) in the presence of thiourea (Fig. 27). The resulting N,S-ACS product showed a three-dimensional interconnected honeycomb-like porous structure with a high accessible surface area (1874 m^2 g^{-1}) appropriate for large ion storage and rapid ion transfer. Total N and S contents were 5.11 and 2.86% distributed as pyridinic-N (35%), pyrrolic-N (17%), quaternary-N (29%), and pyridine-N-oxide (19%), and C–S–C and C–SO–C bonding, respectively.

Dopant elements induced structural defects increasing open channels and active sites and enhanced electron transfer (mostly N) and provided a high surface electron density (mostly S). Overall, an electrode fabricated with N,S-ACS delivered a specific capacitance of 404 F g^{-1} at 0.1 A g^{-1} and when assembled in a symmetric flexible solid state supercapacitor, the device offered an energy density of 30 W h kg^{-1} and a power density of 8000 W kg^{-1} (99% capacitance retention after 10 000 cycles in a PVA/KOH gel electrolyte). This performance was promising for commercial applications in large scale energy storage.[260] Another material for supercapacitor electrodes was achieved starting from waste cotton seed husk (CSH). Pyrolysis/activation of CHS powder at 600–800 °C in the presence of KOH provided a 3D honeycomb-like porous carbon (a-CSH) with interconnected hierarchical (micro, meso-, and macro-) porosity and a high specific surface area (1694.1 m^2 g^{-1}). Moreover, a-CSH was nitrogen self-doped (2.62 at%). A symmetric supercapacitor assembled with an a-CSH-based electrode exhibited a high specific capacitance of 52 F g^{-1} at 0.5 A g^{-1}, with an energy density of 10.4 W h kg^{-1} at 300 W kg^{-1} (91% capacitance retention following 5000 cycles at 10 A g^{-1}).[261]

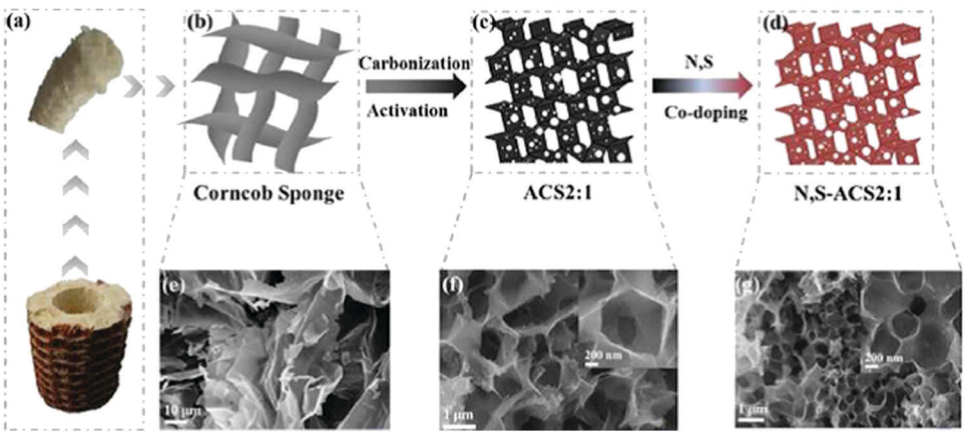

Fig. 27 Fabrication procedure of N,S-ACS materials (top) and their SEM images (bottom). Adapted from ref. 260. Copyright 2018, with permission from the Royal Society of Chemistry.

3.4 Miscellaneous examples

As previously indicated, biowaste is a rich source for the preparation of value-added materials. In addition to already mentioned materials, other products can be obtained from various biowastes.

Among heteroatom-doped carbon materials, nitrogen-doped carbon materials are a relevant class of compounds which find application in different fields including catalysis, electrochemical batteries, energy storage, fuel cells and supercapacitors.[262–264] There are three types of nitrogen (N) with various applications including pyrrolic N, pyridinic N and graphitic N.[265] Recently, the production of these important compounds using chitin and chitosan as eco-friendly, cost effective and available sources has become an attractive topic.[266–272]

Besides the examples detailed in the above paragraphs of Section 3, several other studies on the fabrication of biowaste-derived nanocarbon materials have been described in the recent literature. Table 4 provides a summary of additional relevant examples.

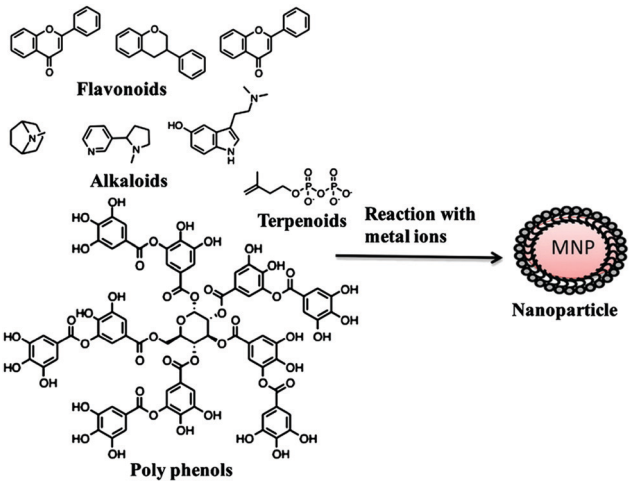

Fig. 28 Common biomolecules in plant extracts for the preparation/stabilization of M-NPs. Adapted from ref. 290. Copyright 2013, with permission from Elsevier.

4. Metal nanoparticles (M-NPs) in colloidal dispersions

The small size of metal nanoparticles (M-NPs) in the range of 1–100 nm, most often below 10 nm, is responsible for an extraordinarily high surface area to volume ratio and large surface energy which explain the capability of M-NPs to adsorb, capture and recognize small molecules at their solid surface. Due to these size- and shape- dependent properties, M-NPs have become increasingly popular in the past twenty years for a variety of applications including biosensing, catalysis, optics, antimicrobial applications, fabrication of computer components, electrometers, *etc.*[287] The large surface energy however is also the reason for the spontaneous tendency of M-NPs to coalesce into thermodynamically favored bulk (large) particles containing less surface atoms with unsaturated bonds. The agglomeration phenomenon is ruled by the Ostwald ripening mechanism through which smaller particles release surface atoms able to diffuse in the solution and to stick to larger particles thereby reducing the total energy of the system.[288] To prevent this, electrostatic, steric and even the combination of these two, named as electrosteric, stabilization modes have been described to provide the spatial confinement of M-NPS by using polymers, surfactants, ionic liquids, solid supports, and ligands with suitable functional groups.[289] Another emerging approach involves protocols based on the use of biomolecules such as proteins/enzymes, flavonoids, polysaccharides, alkaloids, polyphenols, and vitamins, that are present in plant extracts and microbial cells, and may act as both bio-reductants and stabilizers for M-NPs (Fig. 28).[290–292]

With respect to conventional chemical procedures, advantages of such biosynthetic methods include an improved eco-friendly profile because hazardous reductants and solvents (as, for example, hydrazine hydrate, sodium borohydride, and DMF) are avoided, and the production of non-chemically contaminated M-NPs which is relevant to minimize toxicity issues in biomedical applications. In this respect, biowastes are also receiving increasing attention. One of the first examples reported the use of polyphenol-rich red grape pomace as a capping and reducing agent, to fabricate nanoparticles of Ag, Au, Pt, and Pd in aqueous media. In a typical procedure,

Table 4 Biowaste-derived nanocarbon materials

Entry	Biowaste	Prepared nanomaterials	Ref.
1	Sugarcane bagasse pith	Nano-porous activated carbon	273
2	Sago bark	Carbon nanospheres	274
3	Chicken eggshell	Nitrogen-doped fluorescent carbon nanodots	275
4	Coffee grounds	Hierarchically porous carbon nanosheets	276
5	Wood wool	Carbon nano-onions	277
6	Mangosteen peel	Three-dimensional porous carbon	278
7	Rice husk	Carbon nanoparticles	279
8	Amazonian fruits	Activated nanocarbons	280
9	Tea plants	Carbon nanostructures	281
10	*Moringa oleifera* fruit shell extract	Ag-reduced graphene oxide nanocomposite	282
11	Paper pulping	Lignin-based carbon/ZnO nanocomposite	283
12	Pine cone	Pine cone–iron oxide nanocomposites	284
13	Eggshell	Pd/eggshell nanocomposite	285
14	Porcine bone	SnO_2/porcine bone	286

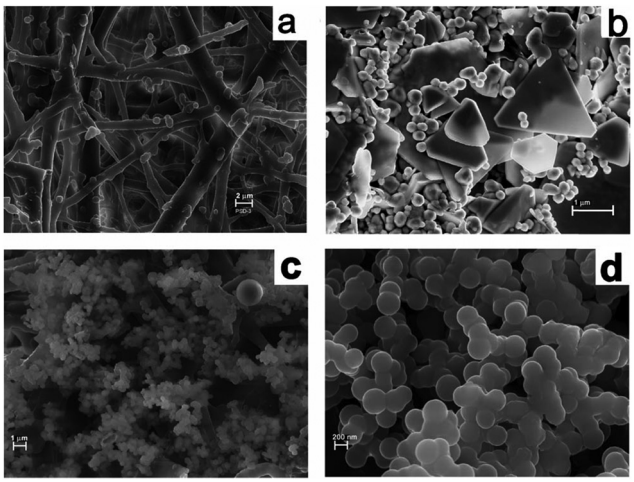

Fig. 29 FESEM images of (a) bare ESM, (b) Au impregnated ESM and (c and d) 80 °C dried membrane showing spherical particles. Adapted from ref. 295. Copyright 2012, with permission from the Royal Society of Chemistry.

a solution of selected metal precursors ($HAuCl_4$, $AgNO_3$, Na_2PdCl_4, and $HPtCl_4$) was added to a pomace extract and microwave heated at 52–55 °C (50 W) for 60 s. Crystalline nanoparticles of Ag, Au, Pt, and Pd were obtained with size around 10, 30, 3–4, and 5–10 nm, respectively, and with variable yields of 80–90%.[293]

A similar approach was used for the bio-reduction of aq. $AgNO_3$ in the presence of mango seed aqueous extracts. The formation of predominantly spherical and hexagonal Ag-NPs of *ca.* 14 nm in size was complete in 30 min at room temperature. In view of exploring the potential for biomedical uses, aqueous mixtures of Ag-NPs and bovine serum albumin (BSA) were examined by fluorescence spectroscopy. The occurrence of a strong interaction between the protein and the metal particles with formation of a ground state complex explained the remarkable quenching observed in the fluorescence of BSA.[294]

Another strategy was conceived starting from a protein-rich membrane (ESM) extracted by mild acid treatment of chicken egg shells. Under ambient conditions, the reaction of ESM with aq. $HAuCl_4$ (0.1 mM–0.1 M) afforded fluorescent Au nanoparticles stabilized either as a colloidal aqueous solution or by adsorption on the membrane. It was hypothesized that amino, carboxyl and carbonyl functionalities constituting the structures of bacteriolytic enzymes (lysozyme and *N*-acetyl glucosaminidase) of the shell membrane acted as both chelating and reducing agents promoting the conversion of aq. Au^{3+} to Au(0) in the NPs. Microstructural (TEM and SEM) and optical investigations proved the formation of particles below 20 nm in the form of pseudo-spheres and triangular prisms (Fig. 29), that displayed intense red and blue emissions at around 630 ± 5 nm and 437 ± 5 nm, respectively, suitable for biolabeling and bioimaging applications.[295]

4.1 Solid supported M-NPs and metal nanocomposites

The stabilization of M-NPs has been conceived through impregnation on solid supports and synthesis of nanocomposites which not only prevent the agglomeration of particles, but offer materials that can be more efficiently handled, *e.g.* for separation from reaction medium in catalysis and/or water disinfection. On this subject, the use of biowastes has inspired different approaches.

One such procedure started from a dispersion of an aqueous solution of $AgNO_3$, ammonia, and glucose dispersed in a mixture of rice husks (RHs) and rice husk ash (RHA). Under alkaline conditions, both deprotonation of silanol groups in RH/RHA and the formation of the silver–ammonia complex, $Ag(NH_3)_2^+$ took place, thereby favoring the adsorption of Ag^+ on the support (Scheme 3, top). The glucose-mediated reduction of metal cations finally provided Ag-NPs of diameters ranging from 10 to 35 nm, impregnated on RH/RHA (atomic silver% in the range of 0.23–0.77) (Scheme 3, bottom).

Ag-NPs on RH/RHA displayed a strong bactericidal effect for both Gram positive (*S. aureus*) and Gram negative (*E. coli*) bacteria, though metal leaching was detected.[296] Rice husk was also used as a starting material for a multistep synthesis of Au-NPs. Furnace calcination at 700 °C of HCl-treated RHs provided silica NPs of *ca.* 60–70 nm, which were functionalized by (3-aminopropyl)-triethoxysilane (APTES). The so-prepared amino-capped silica NPs favored the grafting of aq. $AuCl_4^-$ anions which were reduced by $NaBH_4$, yielding Au-NPs (*ca.* 2–4 nm) immobilized on the silica surface. The overall strategy is shown in Fig. 30. Au-NPs on RH-derived silica exhibited excellent catalytic performance for the 4-nitrophenol (4-NP) hydrogenation to 4-aminophenol, with no loss of activity after three recycles.[297]

A versatile approach for the preparation of lignin-supported NPs of precious metals including Au, Pd, Ru and Re was proposed introducing a bottom-up mechanochemical methodology

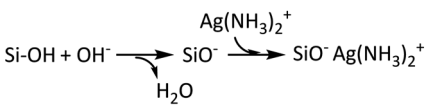

$$2\ OH^- + 2\ [Ag(NH_3)_2^+] + C_6H_{12}O_6 \rightarrow 2\ Ag^0 + 4\ NH_3 + H_2O + C_6H_{12}O_7$$

Scheme 3 Adsorption/reduction of Ag^+ during the impregnation of Ag-NPs on RH/RHA.

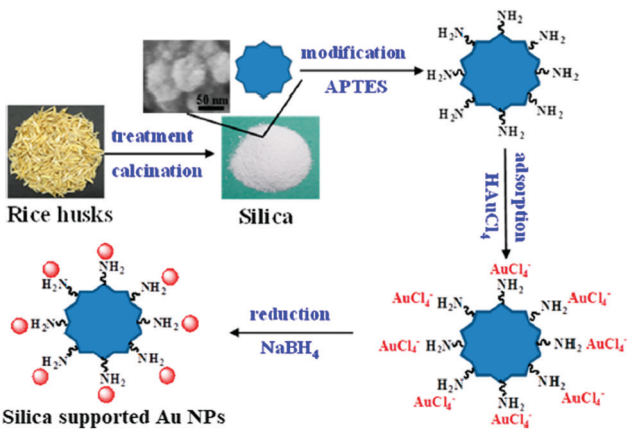

Fig. 30 Preparation of RH-silica-Au NPs. Adapted from ref. 297. Copyright 2015, with permission from ACS.

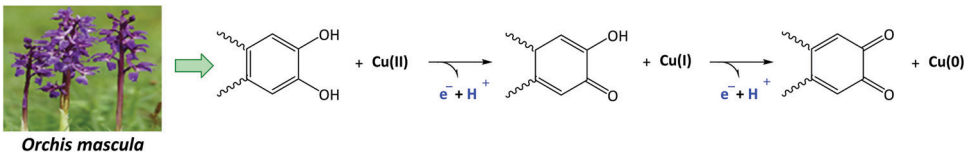

Scheme 4 The bio-reduction of Cu(II) mediated by a polyphenol from *Orchis mascula* extract.

by which a solid mixture of a metal precursor and powdered Kraft lignin was ball-milled in a steel milling jar. Although the reaction mechanism was not elucidated, mechanical breakdown of lignin plausibly brought about the formation of easily oxidizable (poly)-phenolic species which could act as metal reductants. Notably, the incorporation of NPs within lignin was dependent on the nature of the metal precursor with the best results achieved with $HAuCl_4$, $Pd(AcO)_2$ and $Pd(acac)_2$, Ru(III) acetate, and $Re(CO)_5Br$. The corresponding M-NPs were highly monodispersed with a size in the range of 3–6 nm, except for larger Au-NPs of *ca.* 14 nm.[298]

A green synthetic procedure for the fabrication of metal-based nanocomposites was also reported by combining the reducing/stabilizing properties of aqueous extracts from the leaves of *Orchis mascula* L. with the use of a cheap support derived from a largely available biowaste such as chicken egg shells. In a typical reaction, a suspension of powdered egg shells, a metal precursor such as $CuCl_2{\cdot}2H_2O$, $FeCl_3{\cdot}6H_2O$ or their mixture, and an aqueous extract was heated at 70 °C for 3 h. Thereafter, Cu/Fe_3O_4/eggshell, Fe_3O_4/eggshell and Cu/eggshell nanocomposites were recovered by filtration. RP-HPLC-DAD analyses proved that the used aqueous extracts were rich in phenolic and flavonoid compounds (up to 2500–3300 GAE/dried weight of myricetin, caffeic and chlorogenic acids, luteolin 3-*O*-glycoside, kaempferol 7-*O*-glycoside, *etc.*) acting as bio-reductants according to the hypothesis of Scheme 4.

EDX and TEM characterization confirmed that metal amounts and NP sizes were 11.05, 24.69, and 9.80 + 46.32 wt% and 5, 8 and 17 nm for Cu, Fe_3O_4, and Cu/Fe_3O_4, respectively. Under ambient conditions, all nanocomposites proved to be effective catalysts for contaminant dye reduction such as methylene blue (MB), congo red (CR), methyl orange (MO) and rhodamine B (RhB).[299] In a similar approach, an aqueous extract of *Myrica gale* L., a flowering plant of the *Myricaceae* family, was used as a stabilizing and reducing agent for the preparation of Ag-NPs immobilized on a powdered cow bone as a support. SEM and TEM micrographs of the Ag/bone nanocomposite showed that spherical metal NPs of 5–10 nm were distributed on the bone surface (Fig. 31).

The synthesized material exhibited an excellent catalytic performance for the hydrolysis of a variety of arylcyanamides into the corresponding *N*-arylureas, and it could be recycled up to five times with no loss of performance. Notably, the reaction was carried out in *Myrica gale* aqueous extract as a solvent, thereby avoiding the usage of additional media.[300]

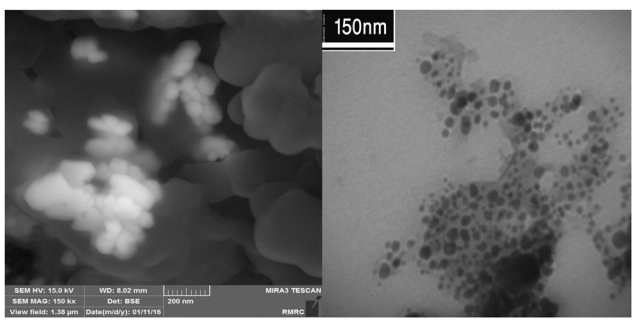

Fig. 31 FESEM (left) and TEM (right) images of the Ag/bone nanocomposite. Adapted from ref. 300. Copyright 2017, with permission from Elsevier.

4.2 Miscellaneous examples

Besides the examples detailed in the above paragraphs of Section 4, several other studies on the synthesis of M-NPs stabilized in suspensions or immobilized on solids derived from biowastes have been described in the recent literature. Table 5 provides a summary of additional relevant examples.

5. Conclusions and future prospects

Biowastes, annually generated at the millions of tonnes scale worldwide, must enter a value chain crucial to rethink the planetary welfare in terms of circular economy, where the concept of sustainable growth has to be implemented through a closed loop for the recycling of any material or its transformation

Table 5 M-NPs stabilized in suspensions or immobilized on solids derived from biowastes

Entry	Biowaste from	Prepared nanomaterials	Application	Ref.
1	Fish scales	Cu NPs	Degradation of methylene blue	301
2	Lignocellulose	Ag NPs	Antibacterial performance against Gram negative organisms	302
3	Banana fruit extract	Au NPs	None	303
4	Vegetables	Au NPs	Antibacterial activity against clinical pathogens	304
5	Food industry	Zero valent Fe NPs	None	305
6	Wine dregs	Au and Ag NPs	None	306
7	Peach kernel shell	Ag NPs	Reduction of MO, 4-NP and MB	307
8	Rice husks	Ru NPs on modified ceria	Benzene hydrogenation	308
9	Chicken eggshell	CaO NPs	Biodiesel production	309
10	Eggshell	$CaCO_3$ nanofibers	None	310

into other resources without harming and/or depleting the natural ecosystem.

Biowastes can be radically transformed, either physically, chemically or biologically, into a broad plethora of end use products and materials. This potential should be assessed on multiple beneficial aspects for the transition to a circular economy, including the design of innovative products, the study of new business and market models, and even the promotion of changes in the consumers' life style and behavior. However, due to the highly heterogeneous nature of biowastes, identifying methods for their valorization is a challenging task not only to conceive the type of end-product or families of end-products, but also to characterize their properties.

This review has been focused on the fabrication of biowaste-derived nanomaterials, starting from a selection of largely available sources such as collagen, chitin and chitosan, hydroxyapatites and bio-silica/silicates, and other C-based feedstocks for bioplastics and nanocarbon structures to be used as such or as supports for metal nanoparticles.

Perspectives for the applications of these materials span most varied sectors from the biomedical area for drug delivery and tissue engineering, to environmental remediation, catalysis, electronics, energy storage, *etc.*, and they are contributing drivers to enhance scientific and technological knowledge in these fields. However, many such investigations are still at an early stage and need to be expanded beyond the discovery of a novel procedure or process, to an in-depth analysis of both technical aspects and socio-ecological boundaries including optimization of purification protocols, extraction yields, up-scaling issues, energy balance and costs, environmental emissions, and public acceptability and approval of new technologies.

Conflicts of interest

The authors declare no competing interest.

Acknowledgements

The support from MINECO under the project CTQ2016-78289-P, co-financed by FEDER funds is gratefully acknowledged. The publication has been prepared with the support of RUDN University, Program 5-100. We also gratefully acknowledge the Iranian Nano Council and the University of Qom for the support of this work.

References

1 D. Weedmark, https://sciencing.com/human-activities-affect-ecosystem-9189.html, updated March 09, 2018.
2 http://ec.europa.eu/environment/waste/compost/index.htm, last updated: 09/06/2016.
3 (*a*) M. M. Tun, D. Juchelková, H. Raclavská and V. Sassmanová, *Energies*, 2018, **11**, 3183; (*b*) http://web.unep.org/ourplanet/september-2015/unep-publications/global-waste-management-outlook.
4 D. Hoornweg and P. Bhada-Tata, *What a Waste: A Global Review of Solid Waste Management*, Urban Development Series Knowledge Papers, The World Bank Group, Washington, DC, USA, 2012, pp. 1–98.
5 *From Waste to Value: Valorisation Pathways for Organic Waste Streams in Circular Bioeconomies*, ed. A. Klitkou and A. Fevolden, Taylor & Francis, 2019.
6 (*a*) J. A. Bennett, K. Wilson and A. F. Lee, *J. Mater. Chem. A*, 2016, **4**, 3617–3637; (*b*) D. Rodriguez-Padron, A. R. Puente-Santiago, A. Caballero, A. M. Balu, A. A. Romero and R. Luque, *Nanoscale*, 2018, **10**, 3961–3968; (*c*) W. Ouyang, J. M. Reina, E. Kuna, A. Yepez, A. M. Balu, A. A. Romero, J. C. Colmenares and R. Luque, *J. Environ. Manage.*, 2017, **203**, 768–773; (*d*) R. Luque, *Curr. Green Chem.*, 2015, **2**, 90–95.
7 (*a*) J. Cai and N. Hishamunda, *FAO Aquacult. Newsl.*, 2013, **51**, 34–36; (*b*) J. Cai and N. Hishamunda, *FAO Aquacult. Newsl.*, 2018, **58**, 49–51.
8 The state of the World fisheries and aquaculture, meeting the sustainable development goals, Food and Agriculture Organization of the United Nations, Rome, 2018, ISBN 978-92-5-130562-1.
9 N. Yan and X. Chen, *Nature*, 2015, **524**, 155–157.
10 G. Caruso, *J. FisheriesSciences.com*, 2016, **10**, 12–015.
11 J. Guillen, S. J. Holmes, N. Carvalho, J. Casey, H. Dörner, M. Gibin, A. Mannini, P. Vasilakopoulos and A. Zanzi, *Sustainability*, 2018, **10**, 900.
12 F. M. Kerton, Y. Liu, K. W. Omari and K. Hawboldt, *Green Chem.*, 2013, **15**, 860–871.
13 K. Jayathilakan, K. Sultana, K. Radhakrishna and A. S. Bawa, *J. Food Sci. Technol.*, 2012, **49**, 278–293.
14 S. Maqsood, S. Benjakul and A. Kamal-Eldin, *Recent Pat. Food, Nutr. Agric.*, 2012, **4**, 141–147.
15 P. Kandra, M. M. Challa and H. K. Jyothi, *Appl. Microbiol. Biotechnol.*, 2012, **93**, 17–29.
16 BBI work plan 2018, topic identifier BBI.2018.SO1.R1: http://ec.europa.eu/research/participants/portal/desktop/en/opportunities/h2020/topics/bbi.2018.so1. r1.html, last access January 24th, 2019.
17 S. L. Wang, T. R. Chen, T. W. Liang and P. C. Wu, *Biochem. Eng. J.*, 2009, **48**, 111–117.
18 A. Alemán, F. González, M. Arancibia, M. E. López-Caballero, P. Montero and M. C. Gómez-Guillén, *Innovative Food Sci. Emerging Technol.*, 2018, **47**, 476–484.
19 W. Yang, Z. Du, Z. Ma, G. Wang, H. Baic and G. Shao, *RSC Adv.*, 2016, **6**, 3942–3950.
20 X. Liu, C. He, X. Yu, Y. Bai, L. Ye, B. Wang and L. Zhang, *Powder Technol.*, 2018, **326**, 181–189.
21 M. N. Kumar, *React. Funct. Polym.*, 2000, **45**, 1–27.
22 J. M. Oliveira Cavalheiro, E. Oliveira de Souza and P. S. Bora, *Bioresour. Technol.*, 2007, **98**, 602–606.
23 M. Ahmaruzzaman, *Prog. Energy Combust. Sci.*, 2010, **36**, 327–363.
24 J. M. Kurola, M. Arnold, M. H. Kontro, M. Talves and M. Romantschuk, *Bioresour. Technol.*, 2011, **102**, 5214–5220.
25 H. Raclavska, D. Juchelkova, V. Roubicek and D. Matysek, *Fuel Process. Technol.*, 2011, **92**, 13–20.

26 J. Zuwala and M. Sciazko, *Biomass Bioenergy*, 2010, **34**, 1165–1174.
27 Z. Gogebakan, Y. Gogebakan, N. Selçuk and E. Selçuk, *Bioresour. Technol.*, 2009, **100**, 1033–1036.
28 N. M. Sigvardsen and L. M. Ottosen, *Cem. Concr. Compos.*, 2019, **95**, 25–32.
29 Z. T. Yao, X. S. Ji, P. K. Sarker, J. H. Tang, L. Q. Ge, M. S. Xia and Y. Q. Xi, *Earth-Sci. Rev.*, 2015, **141**, 105–121.
30 G. Xu and X. Shi, *Resour., Conserv. Recycl.*, 2018, **136**, 95–109.
31 A. Dindi, D. V. Quang, L. F. Vega, E. Nashef and M. R. M. Abu-Zahra, *J. CO_2 Util.*, 2019, **29**, 82–102.
32 M. Visa, L. Andronic and A. Duta, *J. Environ. Manage.*, 2015, **150**, 336–343.
33 N. Salah, A. Alshahrie, N. D. Alharbi, M. S. Abdel-wahab and Z. H. Khan, *J. Mater. Res. Technol.*, 2019, **8**, 250–258.
34 Z. Chen, J. Xing, Z. Pu, X. Wang, S. Yang, B. Wei, Y. Ai, X. Li, D. Chen and X. Wang, *J. Mol. Liq.*, 2018, **266**, 824–833.
35 N. Salah, M. Sh. Abdel-wahab, A. Alshahrie, N. D. Alharbi and Z. H. Khan, *RSC Adv.*, 2017, **7**, 40295–40302.
36 J. Muthu, P. Bradley, I. I. Jinasena, S. Durbach, A. Moya and R. Paskaramoorthy, *Polym. Compos.*, 2018, **39**, 318–328.
37 N. Hintsho, A. Shaikjee, P. K. Triphati, H. Masenda, D. Naidoo, P. Franklyn and S. Durbach, *J. Nanosci. Nanotechnol.*, 2016, **16**, 4672–4683.
38 H. Chen, Applications of Lignocellulose Biotechnology in Other Industries, *Biotechnology of Ligno-cellulose*, Springer, Dordrecht, 2014.
39 *Lignocellulosic Biomass Production and Industrial Applications*, ed. A. Kuila and V. Sharma, Scrivener Publishing, Wiley, 2017.
40 J.-Y. Kim, H. W. Lee, S. M. Lee, J. Jae and Y.-K. Park, *Bioresour. Technol.*, 2019, **279**, 373–384.
41 H. Chen, J. Liu, X. Chang, D. Chen, Y. Xue, P. Liu, H. Lin and S. Han, *Fuel Process. Technol.*, 2017, **160**, 196–206.
42 J. Ma, S. Shi, X. Jia, F. Xia, H. Ma, J. Gao and J. Xu, *J. Energy Chem.*, 2019, **36**, 74–86.
43 B. Padrino, M. Lara-Serrano, S. Morales-delaRosa, J. M. Campos-Martín, J. L. García Fierro, F. Martínez, J. A. Melero and D. Puyol, *Front. Bioeng. Biotechnol.*, 2018, **6**, 119.
44 A. Duque, P. Manzanares and M. Ballesteros, *Renewable Energy*, 2017, **114**, 1427–1441.
45 W. Jianga, A. Kumar and S. Adamopoulos, *Ind. Crops Prod.*, 2018, **124**, 325–342.
46 A. Bhalla, N. Bansal, S. Kumar, K. M. Bischoff and R. K. Sani, *Bioresour. Technol.*, 2013, **128**, 751–759.
47 A. Karnaouri, I. Antonopoulou, A. Zerva, M. Dimarogona, E. Topakas, U. Rova and P. Christakopoulos, *Bioresour. Technol.*, 2019, **279**, 362–372.
48 G. Gogoi and S. Hazarika, *Sep. Purif. Technol.*, 2017, **173**, 113–120.
49 A. Brandt, J. Gräsvik, J. P. Hallett and T. Welton, *Green Chem.*, 2013, **15**, 550–583.
50 S. Sohni, S. A. Khan, K. Akhtar, S. B. Khan, A. M. Asiri, R. Hashim and A. K. Mohd Omar, *Colloids Surf., A*, 2018, **549**, 184–195.
51 L. Zhao, X. Zhang, J. Xu, X. Ou, S. Chang and M. Wu, *Energies*, 2015, **8**, 4096–4117.
52 D. Klein-Marcuschamer, P. Oleskowicz-Popiel, B. A. Simmons and H. W. Blanch, *Biotechnol. Bioeng.*, 2012, **109**, 1083–1087.
53 E. Gnansounou and A. Dauriat, *Bioresour. Technol.*, 2010, **101**, 4980–4991.
54 D. M. Alonso, S. H. Hakim, S. Zhou, W. Won, O. Hosseinaei, J. Tao, V. Garcia-Negron, A. H. Motagamwala, M. A. Mellmer, K. Huang, C. J. Houtman, N. Labbé, D. P. Harper, C. T. Maravelias, T. Runge and J. A. Dumesic, *Sci. Adv.*, 2017, **3**, e1603301.
55 F. G. Gachango, K. S. Ekmann, J. Frørup and S. M. Pedersen, *Aquaculture*, 2017, **479**, 265–272.
56 A. W. Lipkowski, B. Gajkowska, A. Grabowska and K. Kurzepa, *Polimery*, 2009, **54**, 386–388.
57 M. Gonzalo, C. M. Jespersen, K. Jensen, S. Støier and L. Meinert 62nd International Congress of Meat Science and Technology, 14–19th August 2016, Bangkok, Thailand.
58 http://www1.bio.ku.dk/projects/keratin2protein/, last access January 25, 2019.
59 M.-H. Wonga, W.-Y. Mo, W.-M. Choi, Z. Cheng and Y.-B. Man, *Environ. Pollut.*, 2016, **219**, 631–638.
60 Nitrogen inputs to agricultural soils from livestock manure, New statistics, Integrated Crop Management, FAO, Rome, vol. 24, 2018, ISBN 978-92-5-130024-4.
61 I. M. Nasir, T. I. Mohd Ghazi and R. Omar, *Eng. Life Sci.*, 2012, **12**, 258–269.
62 E. Monteiro, V. Mantha and A. Rouboa, *Renewable Energy*, 2011, **36**, 627–631.
63 C. Cavinato, F. Fatone, D. Bolzonella and P. Pavan, *Bioresour. Technol.*, 2010, **101**, 545–550.
64 C. Zhang, G. Xiao, L. Peng, H. Su and T. Tan, *Bioresour. Technol.*, 2013, **129**, 170–176.
65 L. Castrillón, Y. Fernández-Nava, P. Ormaechea and E. Marañón, *Bioresour. Technol.*, 2013, **127**, 312–317.
66 H. Tian, N. Duan, C. Lin, X. Li and M. Zhong, *J. Biosci. Bioeng.*, 2015, **120**, 51–57.
67 S. A. Neshat, M. Mohammadi, G. D. Najafpour and P. Lahijani, *Renewable Sustainable Energy Rev.*, 2017, **79**, 308–322.
68 S. Astals, R. Musenze, X. Bai, S. Tannock, S. Tait, S. Pratt and P. D. Jensen, *Bioresour. Technol.*, 2015, **181**, 97–104.
69 S. Yin, R. Dolan, M. Harris and Z. Tan, *Bioresour. Technol.*, 2010, **101**, 3657–3664.
70 A. Dimitriadis and S. Bezergianni, *Renewable Sustainable Energy Rev.*, 2017, **68**, 113–125.
71 C. Pituello, O. Francioso, G. Simonetti, A. Pisi, A. Torreggiani, A. Berti and F. Morari, *J. Soils Sediments*, 2015, **15**, 792–804.
72 http://www.worldbank.org/en/topic/urbandevelopment/brief/solid-waste-management, last access, January 30, 2019.
73 D. Hoornweg and P. Bhada-Tata, *What a waste, A Global Review of Solid Waste Management*, Urban Development Series, World Bank, Washington, DC USA, 2012, ch. 5.
74 S. Suthar and P. Singh, *Sustainable Cities Soc.*, 2015, **14**, 56–63.
75 B. A. Hakami and E.-S. Sedek Abu Seif, *Int. Res. J. Environ. Sci.*, 2015, **4**, 1–10.

76 P. Williams. The composition of household waste at the kerbside in 2014-15, Zero Waste Scotland, zerowastescotland.org.uk/content/contact-form, last access, January 30, 2019.
77 E. Imbert, *Open Agric.*, 2017, **2**, 195–204.
78 R. Arneil, D. Arancon, C. S. K. Lin, K. M. Chan, T. H. Kwan and R. Luque, *Energy Sci. Eng.*, 2013, **1**, 53–71.
79 F. Girotto, L. Alibardi and R. Cossu, *Waste Manage.*, 2015, **45**, 32–41.
80 T. I. J. Dugmore, J. H. Clark, J. Bustamante, J. A. Houghton and A. S. Matharu, *Top. Curr. Chem.*, 2017, **375**, 46.
81 S. N. Påledal, E. Hellman and J. Moestedt, *Waste Manage.*, 2018, **71**, 636–643.
82 V. dos Santos, R. N. Brandalise and M. Savaris, *Engineering of Biomaterials, Biomaterials: Characteristics and Properties*, Springer AG, 2017.
83 J. Park and R. S. Lakes, *Biomaterials: An Introduction*, Springer Science & Business Media, 2007.
84 M. C. Gómez-Guillén, B. Giménez, M. E. López-Caballero and M. P. Montero, *Food Hydrocolloids*, 2011, **25**, 1813–1827.
85 O. Pasvolsky, R. Umalsky, Y. Naparstek and A. Y. Hershko, in *Anticollagen Antibodies, Autoantibodies*, ed. Y. Shoenfeld, P. L. Meroni and M. E. Gershwin, Elsevier, 3rd edn, 2014.
86 C. H. Lee, A. Singla and Y. Lee, *Int. J. Pharm.*, 2001, **221**, 1–22.
87 R. Parenteau-Bareil, R. Gauvin and F. Berthod, *Materials*, 2010, **3**, 1863–1887.
88 C. Y. Hsiao, C. H. Chou, H. W. Sun and J. N. Seah, EcoDynamic BioLab, Taipei (TW), US7396912 B2, 2008.
89 T. Nagai and N. Suzuki, *Food Chem.*, 2000, **68**, 277–281.
90 Y. Nomura, H. Sakai, Y. Ishii and K. Shirai, *Biosci., Biotechnol., Biochem.*, 1996, **60**, 2092–2094.
91 K.-M. Song, S. K. Jung, Y. H. Kim, Y. E. Kim and N. H. Lee, *Food Bioprod. Process.*, 2018, **110**, 96–103.
92 G. K. S. Arumugam, D. Sharma, R. M. Balakrishnan and J. B. P. Ettiyappan, *Sustainable Chem. Pharm.*, 2018, **9**, 19–26.
93 N. Muhammad, G. Gonfa, A. Rahim, P. Ahmad, F. Iqbala, F. Sharif, A. S. Khan, F. U. Khan, Z. U. H. Khan, F. Rehman and I. U. Rehman, *J. Mol. Liq.*, 2017, **232**, 258–264.
94 P. G. Kumar, T. Nidheesh, K. Govindaraju, J. Suresh and P. V. Suresh, *J. Sci. Food Agric.*, 2016, **97**, 1451–1458.
95 C. Y. Huang, J. M. Kuo, S. J. Wub and H. T. Tsai, *Food Chem.*, 2016, **190**, 997–1006.
96 C. K. S. Pillai, W. Paul and C. P. Sharma, *Prog. Polym. Sci.*, 2009, **34**, 641–678.
97 G. Margoutidis, V. H. Parsons, C. S. Bottaro, N. Yan and F. M. Kerton, *ACS Sustainable Chem. Eng.*, 2018, **6**, 1662–1669.
98 L. G. Baker, C. A. Specht, M. J. Donlin and J. K. Lodge, *Eukaryotic Cell*, 2007, **6**, 855–867.
99 A. Verlee, S. Mincke and C. V. Stevens, *Carbohydr. Polym.*, 2017, **164**, 268–283.
100 R. Devi and R. Dhamodharan, *ACS Sustainable Chem. Eng.*, 2018, **6**, 846–853.
101 H. Yang, G. Gözaydın, R. R. Nasaruddin, J. R. Gerald Har, X. Chen, X. Wang and N. Yan, *ACS Sustainable Chem. Eng.*, 2019, **7**, 5532–5542.
102 C. Peniche, W. Argüelles-Monal and F. M. Goycoolea, Chitin and Chitosan: Major Sources, Properties and Applications, in *Monomers, Polymers and Composites from Renewable Resources*, ed. M. N. Belgacem and A. Gandini, Elsevier, 2008.
103 R. Jayakumar, M. Prabaharan, P. T. Sudheesh Kumar, S. V. Nair and H. Tamura, *Biotechnol. Adv.*, 2011, **29**, 322–337.
104 S. Gopi, P. Balakrishnan, C. Divya, S. Valic, E. G. Bajsic, A. Pius and S. Thomas, *New J. Chem.*, 2017, **41**, 12746–12755.
105 C. C. Satam, C. W. Irvin, A. W. Lang, J. C. R. Jallorina, M. L. Shofner, J. R. Reynolds and J. Carson Meredith, *ACS Sustainable Chem. Eng.*, 2018, **6**, 10637–10644.
106 F. Ding, H. Deng, Y. Du, X. Shi and Q. Wang, *Nanoscale*, 2014, **6**, 9477–9493.
107 Y. Zou and E. Khor, *Carbohydr. Polym.*, 2009, **77**, 516–525.
108 E. Castagnino, M. F. Ottaviani, M. Cangiotti, M. Morelli, L. Casettari and R. A. Muzzarelli, *Carbohydr. Polym.*, 2008, **74**, 640–647.
109 H. Liu, Q. Yang, L. Zhang, R. Zhuo and X. Jiang, *Carbohydr. Polym.*, 2016, **137**, 600–607.
110 N. Pacheco, M. Garnica-Gonzalez, M. Gimeno, E. Bárzana, S. Trombotto, L. David and K. Shirai, *Biomacromolecules*, 2011, **12**, 3285–3290.
111 R. S. C. M. de Queiroz Antonino, B. R. P. L. Fook, V. A. de Oliveira Lima, R. Í. de Farias Rached, E. P. N. Lima, R. J. da Silva Lima, C. A. P. Covas and M. V. L. Fook, *Mar. Drugs*, 2017, **15**, 141.
112 X. Chen, H. Yang, Z. Zhong and N. Yan, *Green Chem.*, 2017, **19**, 2783–2792.
113 E. Khor and L. Y. Lim, *Biomaterials*, 2003, **24**, 2339–2349.
114 V. K. Thakur and M. K. Thaku, *ACS Sustainable Chem. Eng.*, 2014, **2**, 2637–2652.
115 I. Younes and M. Rinaudo, *Mar. Drugs*, 2015, **13**, 1133–1174.
116 P. Kanmani, J. Aravind, M. Kamaraj, P. Sureshbabu and S. Karthikeyan, *Bioresour. Technol.*, 2017, **242**, 295–303.
117 A. Rajeswari, A. Amalraj and A. Pius, *J. Water Process Eng.*, 2016, **9**, 123–134.
118 J. Liang, H. Yan, P. Puligundla, X. Gao, Y. Zhou and X. Wan, *Food Hydrocolloids*, 2017, **69**, 286–292.
119 Y. Yan, X. Zhang, C. Li, Y. Huanga, Q. Dinga and X. Pang, *Appl. Surf. Sci.*, 2015, **332**, 62–69.
120 A. Szcześ, L. Hołysz and E. Chibowski, *Adv. Colloid Interface Sci.*, 2017, **249**, 321–330.
121 M. Akram, R. Ahmed, I. Shakir, W. Aini, W. Ibrahim and R. Hussain, *J. Mater. Sci.*, 2014, **49**, 1461–1475.
122 N. A. M. Barakat, M. S. Khil, A. M. Omran, F. A. Sheikh and H. Y. Kim, *J. Mater. Process. Technol.*, 2009, **209**, 3408–3415.
123 S. Kongsri, K. Janpradit, K. Buapa, S. Techawongstien and S. Chanthai, *Chem. Eng. J.*, 2013, **215–216**, 522–532.
124 W. Pon-On, P. Suntornsaratoon, N. Charoenphandhu, J. Thongbunchoo, N. Krishnamra and I. M. Tang, *Mater. Sci. Eng., C*, 2016, **62**, 183–189.
125 B. Ratna Sunil and M. Jagannatham, *Mater. Lett.*, 2016, **185**, 411–414.
126 P. Shi, M. Liu, F. Fan, C. Yu, W. Lu and M. Du, *Mater. Sci. Eng., C*, 2018, **90**, 706–712.

127 F. Heidari, M. E. Bahrololoom, D. Vashaee and L. Tayebi, *Ceram. Int.*, 2015, **41**, 3094–3100.
128 S. Pokhrel, *Adv. Chem. Eng. Sci.*, 2018, **8**, 225–240.
129 A. Fihri, C. Len, R. S. Varma and A. Solhy, *Adv. Chem. Eng. Sci.*, 2017, **347**, 48–76.
130 K. Mori, T. Hara, M. Oshiba, T. Mizugaki, K. Ebitani and K. Kaneda, *New J. Chem.*, 2005, **29**, 1174–1181.
131 N. Jamwal, M. Gupta and S. Paul, *Green Chem.*, 2008, **10**, 999–1003.
132 M. L. Kantam, K. B. Shiva Kumar, P. Srinivas and B. Sreedhar, *Adv. Synth. Catal.*, 2007, **349**, 1141–1149.
133 S. Sebti, R. Tahir, R. Nazih, A. Saber and S. Boulaajaj, *Appl. Catal., A*, 2002, **228**, 155–159.
134 Y. Zhang, Y. Zhao and C. Xia, *J. Mol. Catal. A: Chem.*, 2009, **306**, 107–112.
135 S. Mallouk, K. Bougrin, A. Laghzizil and R. Benhida, *Molecules*, 2010, **15**, 813–823.
136 M. K. Pillai, S. Singh and S. B. Jonnalagadda, *Synth. Commun.*, 2010, **40**, 3710–3715.
137 S. Sebti, A. Solhy, R. Tahir and A. Smahi, *Appl. Catal., A*, 2002, **235**, 273–281.
138 M. Zahouily, Y. Abrouki, B. Bahlaouan, A. Rayadh and S. Sebti, *Catal. Commun.*, 2003, **4**, 521–524.
139 M. Zahouily, W. Bahlaouan, B. Bahlaouan, A. Rayadh and S. Sebti, *ARKIVOC*, 2005, **xiii**, 150–161.
140 R. Tahir, K. Banert, A. Solhy and S. Sebti, *Appl. Catal., A*, 2006, **246**, 39–42.
141 K. Mori, T. Hara, T. Mizugaki, K. Ebitani and K. Kaneda, *J. Am. Chem. Soc.*, 2004, **126**, 10657–10666.
142 K. Yamaguchi, M. Mori, T. Mizugaki, K. Ebitani and K. Kaneda, *J. Am. Chem. Soc.*, 2000, **122**, 7144–7145.
143 K. Mori, S. Kanai, T. Hara, T. Mizugaki, K. Ebitani, K. Jitsukawa and K. Kaneda, *Chem. Mater.*, 2007, **19**, 1249–1256.
144 K. Mori, M. Tano, T. Mizugaki, K. Ebitani and K. Kaneda, *New J. Chem.*, 2002, **26**, 1536–1538.
145 T. Mitsudome, A. Noujima, T. Mizugaki, K. Jitsukawa and K. Kaneda, *Chem. Commun.*, 2009, 5302–5304.
146 B. Zhang, J. Fang, J. Li, J. J. Lau, D. Mattia, Z. Zhong, J. Xie and N. Yan, *Chem. – Asian J.*, 2016, **11**, 532–539.
147 U. R. Pillai and E. Sahle-Demessie, *Appl. Catal., A*, 2004, **26**, 69–77.
148 H. Anmin, L. Ming, C. Chengkang and M. Dali, *J. Mol. Catal. A: Chem.*, 2007, **267**, 79–85.
149 R. M. Mohamed and E. S. Baeissa, *Appl. Catal., A*, 2013, **464**, 218–224.
150 A. Mitsionis, T. Vaimakis, C. Trapalis, N. Todorova, D. Bahnemannc and R. Dillert, *Appl. Catal., B*, 2011, **106**, 398–404.
151 Y. Liu, H. Zhong, L. Li and C. Zhang, *Mater. Res. Bull.*, 2010, **45**, 2036–2039.
152 A. Safavi and S. Momeni, *J. Hazard. Mater.*, 2012, **201**, 125–131.
153 H. Nishikawa and K. Omamiuda, *J. Mol. Catal. A: Chem.*, 2002, **179**, 193–200.
154 R. M. Mohamed and E. Aazam, *Desalin. Water Treat.*, 2013, **51**, 6082–6090.
155 D. Mahajan, B. A. Ganai, R. Lal Sharma and K. K. Kapoor, *Tetrahedron Lett.*, 2006, **47**, 7919–7921.
156 S. Sebti, R. Tahir, R. Nazih and S. Boulaajaj, *Appl. Catal., A*, 2001, **218**, 25–30.
157 T. Mitsudome, Y. Mikami, H. Mori, S. Arita, T. Mizugaki, K. Jitsukawa and K. Kaneda, *Chem. Commun.*, 2009, 3258–3260.
158 A. Solhy, J. H. Clark, R. Tahir, S. Sebti and M. Larzek, *Green Chem.*, 2006, **8**, 871–874.
159 K. Wang, G. J. Kennedy and R. A. Cook, *J. Mol. Catal. A: Chem.*, 2009, **298**, 88–93.
160 T. Hara, K. Mori, M. Oshiba, T. Mizugaki, K. Ebitani and K. Kaneda, *Green Chem.*, 2004, **6**, 507–509.
161 M. Sudhakar, M. L. Kantam, V. S. Jaya, R. Kishore, K. V. Ramanujachary and A. Venugopal, *Catal. Commun.*, 2014, **50**, 101–104.
162 L. Huang, P. Luo, W. Pei, X. Liu, Y. Wang, J. Wang, W. Xing and J. Huang, *Adv. Synth. Catal.*, 2012, **354**, 2689–2694.
163 J. Fang, J. Li, B. Zhang, X. Yuan, H. Asakura, T. Tanaka, K. Teramura, J. Xie and K. N. Yan, *Nanoscale*, 2015, **7**, 6325–6333.
164 G. Xu, Y. Zhang, Y. Fu and Q. Guo, *ACS Catal.*, 2017, **7**, 1158–1169.
165 Z. Boukha, J. L. Ayastuy, M. Cortés-Reyes, L. J. Alemany, M. A. Gutiérrez-Ortiz and J. R. González-Velasco, *Int. J. Hydrogen Energy*, 2018, **43**, 16949–16958.
166 C. R. Ho, V. Defalque, S. Zheng and A. T. Bell, *ACS Catal.*, 2019, **9**, 2931–2939.
167 Y. Xia, Y. Liu, N. Shi and X. Zhang, *RSC Adv.*, 2019, **9**, 10272–10281.
168 L. Shen, Z. Yu, D. Zhang, H. Yin, C. Wang and A. Wang, *J. Chem. Technol. Biotechnol.*, 2019, **94**, 204–215.
169 K. Usami, K. Xiao and A. Okamoto, *ACS Sustainable Chem. Eng.*, 2019, **7**, 3372–3377.
170 T. Iwata, *Angew. Chem., Int. Ed.*, 2015, **54**, 3210–3215.
171 OECD, 2013, Policies for Bioplastics in the Context of a Bioeconomy, http://search.oecd.org/officialdocuments/publicdisplaydocumentpdf/?cote=DSTI/STP/BIO(2013)6/FINAL&docLanguage=En, last access February 11th, 2019.
172 https://www.european-bioplastics.org/global-market-for-bioplastics-to-grow-by-20-percent/, last access February 11th, 2019.
173 P. Morone, V. E. Tartiu and P. Falcone, *J. Cleaner Prod.*, 2015, **90**, 43–54.
174 C. S. Araújo, A. M. C. Rodrigues, M. R. S. Peixoto Joele, E. A. F. Araújo and L. F. H. Lourenço, *Food Pack. Shelf Life*, 2018, **16**, 23–30.
175 I. S. Bayer, S. G. Puyol, J. A. Heredia-Guerrero, L. Ceseracciu, F. Pignatelli, R. Ruffilli, R. Cingolani and A. Athanassiou, *Macromolecules*, 2014, **47**, 5135–5143.
176 G. Perotto, L. Ceseracciu, R. Simonutti, U. C. Paul, S. Guzman-Puyol, T. N. Tran, I. S. Bayer and A. Athanassiou, *Green Chem.*, 2018, **20**, 894–902.
177 T. Mekonnen, P. Mussone, H. Khalil and D. Bressler, *J. Mater. Chem. A*, 2013, **1**, 13379–13398.
178 K. Y. Nandiwale, S. P. Borikar and V. V. Bokade, *Clean: Soil, Air, Water*, 2015, **43**, 927–931.

179 M. Auriemma, A. Piscitelli, R. Pasquino, P. Cerruti, S. Angelini, G. Scarinzi, M. Malinconico and N. Grizzuti, *AIP Conf. Proc.*, 2015, **1965**, 020026.
180 K. W. Lee, J. W. Chung and S.-Y. Kwak, *ACS Sustainable Chem. Eng.*, 2018, **6**, 9006–9017.
181 Y. Yang, J. Huang, R. Zhang and J. Zhu, *Mater. Des.*, 2017, **126**, 29–36.
182 L. A. Derry, A. C. Kurtz, K. Ziegler and O. A. Chadwick, *Nature*, 2005, **433**, 728–731.
183 C. M. Zaremba and G. D. Stucky, *Curr. Opin. Solid State Mater. Sci.*, 1996, **1**, 425–429.
184 FAO, Rice market monitor, http://www.fao.org/3/I9243EN/i9243en.pdf, last access February 14, 2019.
185 W. Wang, J. C. Martin, X. Fan, A. Han, Z. Luo and L. Sun, *ACS Appl. Mater. Interfaces*, 2012, **4**, 977–981.
186 K. G. Patel, R. R. Shettigar and N. M. Misra, *J. Adv. Agric. Technol.*, 2017, **4**, 274–279.
187 Y. Shen, *J. Agric. Food Chem.*, 2017, **65**, 995–1004.
188 S. Praneetha and A. Vadivel Murugan, *ACS Sustainable Chem. Eng.*, 2015, **3**, 224–236.
189 R. Choudhary, S. Koppala and S. Swamiappan, *J. Asian Ceram. Soc.*, 2015, **3**, 173–177.
190 W. You, M. Hong, H. F. Zhang, Q. Wu, Z. Zhuang and Y. Yu, *Phys. Chem. Chem. Phys.*, 2016, **18**, 15564–15573.
191 F. A. Sheikh, M. A. Kanjwal, J. Macossay, M. A. Muhammad, T. Cantu, N. A. M. Barakat and H. Y. Kim, *J. Biomater. Tissue Eng.*, 2011, **1**, 194–197.
192 J. Wasswa, J. Tang and X. Gu, *Food Rev. Int.*, 2007, **23**, 159–174.
193 M.-M. Chen, Y.-Q. Huang, H. Guo, Y. Liu, J.-H. Wang, J.-L. Wu and Q.-Q. Zhang, *J. Appl. Polym. Sci.*, 2014, **131**, 40998.
194 R. D. Thanoon, R. Subramaniam, E. A. Makky and M. M. Yusoff, *Jordan J. Biol. Sci.*, 2018, **11**, 17–22.
195 H. M. P. M. Jose, P. Murugesan, M. Arumugam and K. Mahesh Kumar, *Int. J. Pharm. Pharm. Sci.*, 2014, **6**, 654–657.
196 P. Terzioğlu, H. Öğüt and A. Kalemtas, *Mater. Sci. Eng., C*, 2018, **91**, 899–911.
197 S. Iswariya, P. Velswamy and T. S. Uma, *J. Polym. Environ.*, 2018, **26**, 2086–2095.
198 E. I. Akpan, S. O. Adeosun, G. I. Lawal, S. A. Balogun and X. D. Chen, *J. Nat. Fibers*, 2016, **13**, 103–124.
199 T. Nagai, E. Yamashita, K. Taniguchi, N. Kanamori and N. Suzuki, *Food Chem.*, 2001, **72**, 425–429.
200 L. Xiaoying, F. Yongbin, G. Dachun and C. Wei, *Key Eng. Mater.*, 2007, **342–343**, 213–216.
201 L. S. Senaratne, P.-J. Park and S.-K. Kim, *Bioresour. Technol.*, 2006, **97**, 191–197.
202 G. S. Kumar and E. K. Girija, *Ceram. Int.*, 2013, **39**, 8293–8299.
203 S. Sankar, S. Sekar, R. Mohan, S. Rani, J. Sundaraseelan and T. P. Sastry, *Int. J. Biol. Macromol.*, 2008, **42**, 6–9.
204 A.-R. Ibrahim, W. Wei, D. Zhang, H. Wang and J. Li, *Mater. Lett.*, 2013, **110**, 195–197.
205 A. Muthuvel, T. Ajithkumar and T. Balasubramanian, *J. Appl. Biol. Sci.*, 2011, **5**, 7–10.
206 W.-K. Liu, B.-S. Liaw, H.-K. Chang, Y.-F. Wang and P.-Y. Chen, *JOM*, 2017, **69**, 713–718.
207 A. Veeruraj, M. Arumugam, T. Ajithkumar and T. Balasubramanian, *J. Mater. Sci.: Mater. Med.*, 2012, **23**, 1729–1738.
208 S. Thammahiwes, S.-A. Riyajan and K. Kaewtatip, *J. Polym. Environ.*, 2018, **26**, 1775–1781.
209 Y.-P. Chen, C.-H. Liang, H.-T. Wu, H.-Y. Pang, C. Chen, G.-H. Wang and L.-P. Chan, *J. Food Sci. Technol.*, 2018, **55**, 2310–2317.
210 K. P. Kota, S. S. Shaik, R. K. Kota and A. P. Karlapudi, *Int. J. Pharm. Sci. Rev. Res.*, 2014, **27**, 373–375.
211 A. B. Muley, S. A. Chaudhari, K. H. Mulchandani and R. S. Singhal, *Int. J. Biol. Macromol.*, 2018, **111**, 1047–1058.
212 S. Thammahiwes, S.-A. Riyajan and K. Kaewtatip, *J. Cereal Sci.*, 2017, **75**, 186–191.
213 T. Kleekayai and W. Suntornsuk, *World J. Microbiol. Biotechnol.*, 2011, **27**, 1145–1154.
214 C.-S. Wu, *Polym. Degrad. Stab.*, 2012, **97**, 64–71.
215 M. Ashokkumar, K. M. Sumukh, R. Murali, N. T. Narayanan, P. M. Ajayan and P. Thanikaivelan, *Carbon*, 2012, **50**, 5574–5582.
216 A. L. Wong, H. Chua, W. H. Lo and P. H. F. Yu, *Water Sci. Technol.*, 2000, **41**, 55–59.
217 S. Kumari, R. Rath, A. S. H. Kumar and T. N. Tiwari, *Environ. Technol. Innovation*, 2015, **3**, 77–85.
218 T. M. A. Moro, J. L. R. Ascheri, J. A. R. Ortiz, C. W. P. Carvalho and A. Meléndez-Arévalo, *Food Bioprocess Technol.*, 2017, **10**, 1798–1808.
219 S.-L. Wang, W.-N. Tseng and T.-W. Liang, *Biodegradation*, 2011, **22**, 939–948.
220 M. Ben, T. Mato, A. Lopez, M. Vila, C. Kennes and M. C. Veiga, *Water Sci. Technol.*, 2011, **63**, 1196–1202.
221 V. L. Pachapur, K. Guemiza, T. Rouissi, S. J. Sarma and S. K. Brar, *J. Chem. Technol. Biotechnol.*, 2016, **91**, 2331–2339.
222 H. Chen, L. Zhao, X. Wang, X. He, W. Fang, X. Wang and F. Wang, *Ceram. Int.*, 2015, **41**, 6089–6097.
223 C. Webster, O. Onokpise, M. Abazinge, J. Muchovej, E. Johnson and C. Louime, *Am. J. Environ. Sci.*, 2014, **10**, 357–362.
224 B. I. Ugheoke and O. Mamat, *Int. J. Mater. Eng. Innovation*, 2012, **3**, 139–155.
225 M.-T. Yen, J.-H. Yang and J.-L. Mau, *Carbohydr. Polym.*, 2009, **75**, 15–21.
226 S. Collazo-Bigliardi, R. Ortega-Toro and A. Chiralt Boix, *Carbohydr. Polym.*, 2018, **191**, 205–215.
227 N. Rakkhumkaew and C. Pengsuk, *Food Sci. Biotechnol.*, 2018, **27**, 1201–1208.
228 B. R. Rampazzo, D. Alkan, S. Gazzotti, M. A. Ortenzi, G. Piva and L. Piergiovanni, *Packag. Technol. Sci.*, 2017, **30**, 645–661.
229 J. Ma, C. Xin and C. Tan, *Int. J. Biol. Macromol.*, 2015, **80**, 547–556.
230 D. Pavan Kumar, M. V. Chandra, K. Elavarasan and B. A. Shamasundar, *Int. J. Food Prop.*, 2017, **20**, S2612–S2625.
231 J. J. Vilatela and D. Eder, *ChemSusChem*, 2012, **5**, 456–478.

232 S. K. Rastogi, A. Kalmykov, N. Johnson and T. Cohen-Karni, *J. Mater. Chem. B*, 2018, **6**, 7159–7178.
233 C. Tang, M.-M. Titirici and Q. Zhang, *J. Energy Chem.*, 2017, **26**, 1077–1093.
234 M. Arugula and A. Simonian, *J. Solid State Sci. Technol.*, 2016, **5**, M3045–M3053.
235 M. Zhang, K. P. Annamalai, L. Liu, T. Chen and Y. Tao, *Recent Innovations Chem. Eng.*, 2016, **9**, 4–19.
236 A. Bhati, G. K. M. Tripathi, A. Singh, S. Sarkar and S. K. Sonkar, *New J. Chem.*, 2018, **42**, 16411–16427.
237 S. D. Lakshmi, P. K. Avti and G. Hegde, *Nano-Struct. Nano-Objects*, 2018, **16**, 306–321.
238 M. Ashokkumar, N. T. Narayanan, A. L. M. Reddy, B. K. Gupta, B. Chandrasekaran, S. Talapatra, P. M. Ajayan and P. Thanikaivelan, *Green Chem.*, 2012, **14**, 1689–1695.
239 M. Ashokkumar, A. C. Chipara, N. T. Narayanan, A. Anumary, R. Sruthi, P. Thanikaivelan, R. Vajtai, S. A. Mani and P. M. Ajayan, *ACS Appl. Mater. Interfaces*, 2016, **8**, 14836–14844.
240 B. Telay Mekonnen, A. Meiyazhagan, M. Ragothaman, C. Kalirajan and T. Palanisamy, *J. Cleaner Prod.*, 2019, **210**, 190–199.
241 E. Thompson, A. E. Danks, L. Bourgeois and Z. Schnepp, *Green Chem.*, 2015, **17**, 551–556.
242 A. Zuliani, M. J. Munoz-Batista and R. Luque, *Green Chem.*, 2018, **20**, 3001–3007.
243 A. Kumar, G. Hegde, S. A. B. A. Manaf, Z. Ngaini and K. V. Sharma, *Chem. Commun.*, 2014, **50**, 12702–12705.
244 G. A. M. Ali, S. A. B. A. Manaf, A. Divyashree, K. F. Chong and G. Hegde, *J. Energy Chem.*, 2016, **25**, 734–739.
245 J. B. Essner and G. A. Baker, *Environ. Sci.: Nano*, 2017, **4**, 1216–1263.
246 R. Wang, K.-Q. Lu, Z.-R. Tang and Y.-J. Xu, *J. Mater. Chem. A*, 2017, **5**, 3717–3734.
247 S. Cailotto, R. Mazzaro, F. Enrichi, A. Vomiero, M. Selva, E. Cattaruzza, D. Cristofori, E. Amadio and A. Perosa, *ACS Appl. Mater. Interfaces*, 2018, **10**, 40560–40567.
248 X. Zhang, M. Jiang, N. Niu, Z. Chen, S. Li, S. Liu and J. Li, *ChemSusChem*, 2018, **11**, 11–24.
249 R. Das, R. Bandyopadhyay and P. Pramanik, *Mater. Today Chem.*, 2018, **8**, 96–109.
250 W. Lu, X. Qin, S. Liu, G. Chang, Y. Zhang, Y. Luo, A. M. Asiri, A. O. A. Youbi and X. Sun, *Anal. Chem.*, 2012, **84**, 5351–5357.
251 W. Du, X. Xu, H. Hao, R. Liu, D. Zhang, F. Gao and Q. Lu, *Sci. China: Chem.*, 2015, **58**, 863–870.
252 G. Wu, M. Feng and H. Zhan, *RSC Adv.*, 2015, **5**, 44636–44641.
253 Z. Wang, J. Yu, X. Zhang, N. Li, B. Liu, Y. Li, Y. Wang, W. Wang, Y. Li and L. Zhang, *ACS Appl. Mater. Interfaces*, 2016, **8**, 1434–1439.
254 R. Liu, J. Zhang, M. Gao, Z. Li, J. Chen, D. Wu and P. Liu, *RSC Adv.*, 2015, **5**, 4428–4433.
255 A. Suryawanshi, M. Biswal, D. Mhamane, R. Gokhale, S. Patil, D. Guin and S. Ogale, *Nanoscale*, 2014, **6**, 11664–11670.
256 Y. Li, W. Liao, Z. Li, T. Feng, L. Sun, C. Guo, J. Zhang and J. Li, *Carbon*, 2017, **125**, 640–648.
257 C. Guo, R. Hu, W. Liao, Z. Li, L. Sun, D. Shi, Y. Li and C. Chen, *Electrochim. Acta*, 2017, **236**, 228–238.
258 P. Yang, J. Xie and C. Zhong, *ACS Appl. Energy Mater.*, 2018, **1**, 616–622.
259 D. Yu, C. Chen, G. Zhao, L. Sun, B. Du, H. Zhang, Z. Li, Y. Sun, F. Besenbacher and M. Yu, *ChemSusChem*, 2018, **11**, 1678–1685.
260 Y. Liu, Z. Xiao, Y. Liu and L.-Z. Fan, *J. Mater. Chem. A*, 2018, **6**, 160–166.
261 H. Chen, G. Wang, L. Chen, B. Dai and F. Yu, *Nanomaterials*, 2018, **8**, 412.
262 M. Inagaki, M. Toyoda, Y. Soneda and T. Morishita, *Carbon*, 2018, **132**, 104–140.
263 J. Wu, Z. Pan, Y. Zhang, B. Wang and H. Peng, *J. Mater. Chem. A*, 2018, **6**, 12932–12944.
264 Y. Deng, Y. Xie, K. Zou and X. Ji, *J. Mater. Chem. A*, 2016, **4**, 1144–1173.
265 Q. Lv, W. Si, J. He, L. Sun, C. Zhang, N. Wang, Z. Yang, X. Li, X. Wang, W. Deng, Y. Long, C. Huang and Y. Li, *Nat. Commun.*, 2018, **9**, 3376.
266 S. Zheng, Y. Cui, J. Zhang, Y. Gu, X. Shi, C. Peng and D. Wang, Carbon, *RSC Adv.*, 2019, **9**, 10976–10982.
267 C. J. Raj, M. Rajesh, R. Manikandan, K. H. Yu, J. R. Anusha, J. H. Ahn, D.-W. Kim, S. Y. Park and B. C. Kim, *J. Power Sources*, 2018, **386**, 66–76.
268 S. Kumar, S. T. Aziz, O. Girshevitz and G. D. Nessim, *J. Phys. Chem. C*, 2018, **122**, 2343–2349.
269 R. Hao, Y. Yang, H. Wang, B. Jia, G. Ma, D. Yu, L. Guo and S. Yang, *Nano Energy*, 2018, **45**, 220–228.
270 J. Cheng, Q. Xu, X. Wang, Z. Li, F. Wu, J. Shao and H. Xie, *Sustainable Energy Fuels*, 2019, **3**, 1215–1224.
271 Y. Zhang, L. Lu, S. Zhang, Z. Lv, D. Yang, J. Liu, Y. Chen, X. Tian, H. Jin and W. Song, *J. Mater. Chem. A*, 2018, **6**, 5740–5745.
272 Y. Gao, X. Chen, J. Zhang and N. Yan, *ChemPlusChem*, 2015, **80**, 1556–1564.
273 A. Jain and S. K. Tripathi, *J. Energy Storage*, 2015, **4**, 121–127.
274 G. Hegde, S. A. A. Manaf, A. Kumar, G. A. M. Ali, K. F. Chong, Z. Ngaini and K. V. Sharma, *ACS Sustainable Chem. Eng.*, 2015, **3**, 2247–2253.
275 Y. Ke, B. Garg and Y.-C. Ling, *RSC Adv.*, 2014, **4**, 58329–58336.
276 Y. S. Yun, M. H. Park, S. J. Hong, M. E. Lee, Y. W. Park and H.-J. Jin, *ACS Appl. Mater. Interfaces*, 2015, **7**, 3684–3690.
277 S. K. Sonkar, M. Roy, D. G. Babar and S. Sarkar, *Nanoscale*, 2012, **4**, 7670–7675.
278 Y. Li, X. Wang and M. Cao, *J. CO_2* Util., 2018, **27**, 204–216.
279 P. Z. Z. Ngu, S. P. P. Chia, J. F. Y. Fong and S. M. Ng, *New Carbon Mater.*, 2016, **31**, 135–143.
280 O. F. Cruz, J. Silvestre-Albero, M. E. Casco, D. Hotza and C. R. Rambo, *Mater. Chem. Phys.*, 2018, **216**, 42–46.
281 Ö. Güler, M. Boyrazlı, Ö. Başgöz and B. Bostancı, *Can. Metall. Q.*, 2017, **56**, 349–359.
282 P. O. Patil, P. V. Bhandari, P. K. Deshmukh, S. S. Mahale, A. G. Patil, H. R. Bafna, K. V. Patel and S. B. Bari, *Res. Chem. Intermed.*, 2017, **43**, 3757–3773.

283 H. Wang, X. Qiu, R. Zhong, F. Fu, Y. Qian and D. Yang, *Mater. Chem. Phys.*, 2017, **199**, 193–202.
284 I. L. A. Ouma, E. B. Naidoo and A. E. Ofomaja, *Eur. Phys. J.: Appl. Phys.*, 2017, **79**, 30401.
285 M. Khazaei, A. Khazaei, M. Nasrollahzadeh and M. R. Tahsil, *Tetrahedron*, 2017, **73**, 5613–5623.
286 Y. Wu, H. Wang, M. Cao, Y. Zhang, F. Cao, X. Zheng, J. Hu, J. Dong and Z. Xiao, *J. Nanosci. Nanotechnol.*, 2015, **15**, 6495–6502.
287 Y. Dahman, *Nanotechnology and Functional Materials for Engineers, Nanoparticles*, Elsevier, 2017, ch. 5.
288 M. Selva, A. Perosa and P. Canton, *Curr. Org. Chem.*, 2017, **21**, 2445–2454.
289 A. Kraynov and T. E. Müller, in *Concepts for the Stabilization of Metal Nanoparticles in Ionic Liquids, Applications of Ionic Liquids in Science and Technology*, ed. S. Handy, Intech, 2011.
290 A. K. Mittal, Y. Chisti and U. C. Banerjee, *Biotechnol. Adv.*, 2013, **31**, 346–356.
291 N. Asmathunisha and K. Kathiresan, *Colloids Surf., B*, 2013, **103**, 283–287.
292 S. Iravani, *Green Chem.*, 2011, **13**, 2638–2650.
293 B. Baruwati and R. S. Varma, *ChemSusChem*, 2009, **2**, 1041–1044.
294 T. V. M. Sreekanth, S. Ravikumar and Y. R. Lee, *J. Mol. Recognit.*, 2016, **29**, 253–259.
295 P. S. Devi, S. Banerjee, S. R. Chowdhury and G. S. Kumar, *RSC Adv.*, 2012, **2**, 11578–11585.
296 D. He, A. Ikeda-Ohno, D. D. Boland and T. D. Waite, *Environ. Sci. Technol.*, 2013, **47**, 5276–5284.
297 Y. Li, J. Y. Lan, J. Liu, J. Yu, Z. Luo, W. Wang and L. Sun, *Ind. Eng. Chem. Res.*, 2015, **54**, 5656–5663.
298 M. J. Rak, T. Friščić and A. Moores, *Faraday Discuss.*, 2014, **170**, 155–167.
299 M. Nasrollahzadeh, S. M. Sajadi and A. Hatamifard, *Appl. Catal., B*, 2016, **191**, 209–227.
300 S. S. Momeni, M. Nasrollahzadeh and A. Rustaiyan, *J. Colloid Interface Sci.*, 2017, **499**, 93–101.
301 T. Sinha and M. Ahmaruzzaman, *Environ. Sci. Pollut. Res.*, 2015, **22**, 20092–20100.
302 V. P. Manjamadha and K. Muthukumar, *Int. J. Nanosci.*, 2016, **15**, 1660001.
303 G. K. Deokar and A. G. Ingale, *RSC Adv.*, 2016, **6**, 74620–74629.
304 R. Mythili, T. Selvankumar, P. Srinivasan, A. Sengottaiyan, J. Sabastinraj, F. Ameen, A. Al-Sabri, S. Kamala-Kannan, M. Govarthanan and H. Kim, *J. Mol. Liq.*, 2018, **262**, 318–321.
305 S. Machado, J. P. Grosso, H. P. A. Nouws, J. T. Albergaria and C. Delerue-Matos, *Sci. Total Environ*, 2014, **496**, 233–240.
306 N. González-Ballesteros, J. B. Rodríguez-González and M. C. Rodríguez-Argüelles, *J. Photochem. Photobiol., B*, 2018, **178**, 302–309.
307 B. Khodadadi, M. Bordbar and M. Nasrollahzadeh, *J. Colloid Interface Sci.*, 2017, **493**, 85–93.
308 O. B. Shawkataly, R. Jothiramalingam, F. Adam, T. Radhika, T. M. Tsao and M. K. Wang, *Catal. Sci. Technol.*, 2012, **2**, 538–546.
309 P. R. Pandit and M. H. Fulekar, *J. Environ. Manage.*, 2017, **198**, 319–329.
310 A. Tavangar, B. Tan and K. Venkatakrishnan, *J. Nanobiotechnol.*, 2011, **9**, 1.

